iScience

CellPress
OPEN ACCESS

Article

Upstream ORFs Prevent MAVS Spontaneous Aggregation and Regulate Innate Immune Homeostasis

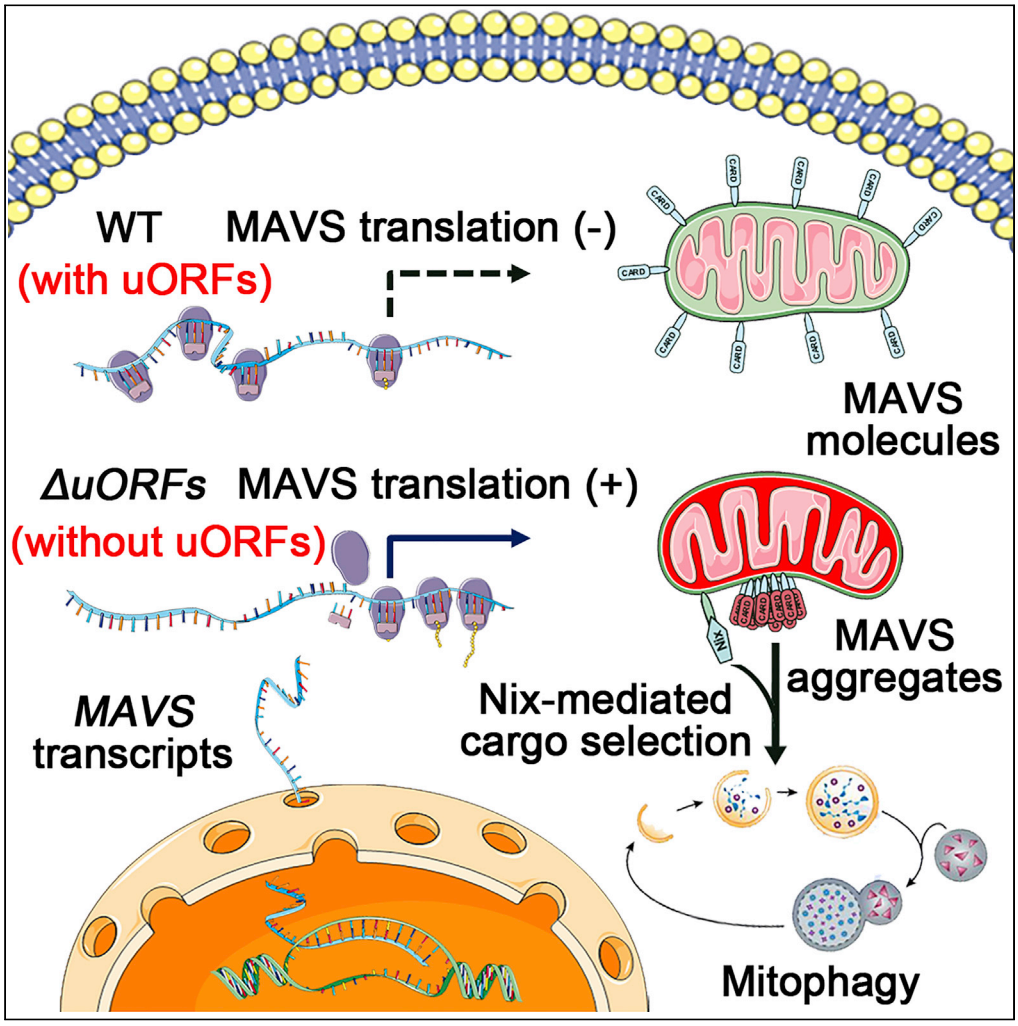

Yuheng Shi, Jing Wu, Tiansheng Zhong, ..., Wei Du, Bang-Ce Ye, Nan Qi

qinan@zjut.edu.cn

HIGHLIGHTS

uORFs are safety checks preventing MAVS spontaneous aggregation and auto-activation

uORFs exert the quantity and quality control of MAVS

Spontaneously aggregated MAVS induces an antiviral state in quiescent cells

Nix mediates the cargo selection and mitophagic clearance of MAVS aggregates

Shi et al., iScience 23, 101059
May 22, 2020
https://doi.org/10.1016/j.isci.2020.101059

iScience

CellPress
OPEN ACCESS

Article

Upstream ORFs Prevent MAVS Spontaneous Aggregation and Regulate Innate Immune Homeostasis

Yuheng Shi,[1,2] Jing Wu,[1] Tiansheng Zhong,[1] Wenting Zhu,[3] Guolan She,[1] Hao Tang,[1] Wei Du,[1] Bang-Ce Ye,[1] and Nan Qi[1,4,*]

SUMMARY

The monomer-to-filament transition of MAVS is essential for the RIG-I/MDA5-mediated antiviral signaling. In quiescent cells, monomeric MAVS is under strict regulation for preventing its spontaneous aggregation, which would result in dysregulated interferon (IFN-α/β) production and autoimmune diseases like systemic lupus erythematosus. However, the detailed mechanism by which MAVS is kept from spontaneous aggregation remains largely unclear. Here, we show that upstream open reading frames (uORFs) within the *MAVS* transcripts exert a post-transcriptional regulation for preventing MAVS spontaneous aggregation and auto-activation. Mechanistically, we demonstrate that uORFs are *cis*-acting elements initiating leaky ribosome scanning of the downstream ORF codons, thereby repressing the full-length MAVS translation. We further uncover that endogenous MAVS generated from the uORF-deprived transcript spontaneously aggregates, triggering the Nix-mediated mitophagic clearance of damaged mitochondria and aggregated MAVS. Our findings reveal the uORF-mediated quantity and quality control of MAVS, which prevents aberrant protein aggregation and maintains innate immune homeostasis.

INTRODUCTION

Sensing of pathogenic microbes by the innate immune system promotes host defense. Host cells employ various pattern recognition receptors (PRRs), including Toll-like receptors, RIG-I-like receptors, Nod-like receptors, and cGAS to detect common pathogenic molecular features, thereby initiating signal transduction (Lee and Kim, 2007; Sun et al., 2013; Takeuchi and Akira, 2010). Activation of signaling cascades through PRR-adaptor pairs results in the production of type I interferons (IFNs), which are secreted to induce the expression of interferon-stimulated genes (ISGs) and eventually establish an antiviral state for virus clearance (Sharma et al., 2003). Apart from its important role in initiating proper antiviral immune responses, activation of the IFN pathway has been implicated in the pathogenesis of many autoimmune disorders like systemic lupus erythematosus (SLE) (Ronnblom, 2011). Therefore, precise regulation of the IFN signaling pathway is of great significance for both eliminating virus and maintaining cellular homeostasis.

Mitochondria have emerged as vital platforms for antiviral signaling. This is largely due to the mitochondrial location of MAVS (also known as VISA, IPS-1, Cardif), an adaptor protein receiving antiviral signal from two independent cytosolic PRRs RIG-I/MDA5 (Kawai et al., 2005; Meylan et al., 2005; Seth et al., 2005; Xu et al., 2005). Upon virus infection, RIG-I senses viral RNA and recruits MAVS through CARD-CARD interaction, which induces inactive MAVS monomers to form active prion-like aggregates (Hou et al., 2011; Xu et al., 2014). The monomer-to-filament transition of MAVS triggers activation of the downstream TBK1/IKKε-IRF3 and IKKα/β-NF-κB signaling cascades, which collaborate to drive the production of type I IFNs and proinflammatory cytokines (Fitzgerald et al., 2003; Zandi et al., 1997). Given its central position and critical role in the antiviral signaling pathway, MAVS is an ideal target by which both host cells and viruses regulate IFN production. In recent years, studies have been focused on the MAVS regulome and have provided considerable insight into how MAVS is regulated under viral infection (Jacobs and Coyne, 2013). In the quiescent cells, however, little is known about the mechanism by which MAVS is kept from spontaneous aggregation. Otherwise, the spontaneous activation of MAVS would induce continuous IFN production and result in detrimental inflammation.

[1]Institute of Engineering Biology and Health, Collaborative Innovation Center of Yangtze River Delta Region Green Pharmaceuticals, College of Pharmaceutical Sciences, Zhejiang University of Technology, Hangzhou, Zhejiang 310014, China

[2]Institutes of Biomedical Sciences, Fudan University, Shanghai 20032, China

[3]Materials Interfaces Center Institute of Advanced Materials Science and Engineering Shenzhen Institutes of Advanced Technology, Chinese Academy of Sciences, Shenzhen 518055, China

[4]Lead Contact

*Correspondence: qinan@zjut.edu.cn

https://doi.org/10.1016/j.isci.2020.101059

Upstream open reading frames (uORFs) are prevalent within the 5′ UTR (leader sequence) of gene transcripts in vertebrates. It was estimated that nearly half of the mammalian transcriptomes contain at least one uORF (49.5% for human and 46.1% for mouse) (Johnstone et al., 2016). Even though most uORFs can be translated, only a few have been found to express a biologically functional peptide (Andrews and Rothnagel, 2014). Emerging evidence shows that many uORFs act in *cis* to repress the translation of downstream ORFs by triggering leaky scanning, reinitiation, and ribosome stalling (Gunišová and Valášek, 2014; Ishimura et al., 2014; Wang and Rothnagel, 2004). uORF presence also correlates with lower steady-state RNA levels, as translation of some uORFs causes nonsense-mediated mRNA decay (Matsui et al., 2007; Mendell et al., 2004). In addition, uORF polymorphism has been found to be associated with a variety of human diseases (Barbosa and Gene, 2014; Calvo et al., 2009; Chatterjee et al., 2010). Functional classes of uORF-containing genes are involved in key cellular processes, such as circadian rhythms, meiosis, and stress response (Brar et al., 2012; Janich et al., 2015; Lawless et al., 2009). However, it remains unclear whether the antiviral signaling molecules undergo uORF-mediated regulation.

In our recent work, a post-translational mechanism for regulation of MAVS was uncovered, showing that the spontaneous aggregation of MAVS is blocked by its multiple truncated isoforms (Qi et al., 2017). Here we dissect a post-transcriptional regulation of MAVS that is mediated by its mRNA-harboring uORFs. MAVS produced from the uORF-deprived transcript is shown to be spontaneously aggregated, thereby activating the IFN signaling pathway and provoking an antiviral state in quiescent human and mouse cells. We further demonstrate that *MAVS* uORFs function as *cis*-acting elements to repress downstream ORF translation by the leaky scanning mechanism. When uORFs are absent in the *MAVS* genomic sequence, the endogenous MAVS forms spontaneous aggregates, which are degraded by the Nix-mediated selective autophagy pathway. Therefore, our findings reveal a regulatory role of uORFs as the quantity and quality control of MAVS, which prevents MAVS spontaneous aggregation and avoids accidental activation of the IFN signaling pathway in the quiescent cells.

RESULTS

Absence of *MAVS* uORFs Leads to Activation of the IFN Signaling Pathway in the Quiescent Cells

MAVS is an adaptor protein essential for the virus-triggered IFN signaling pathway. Although multiple transcript variants have been found for the *MAVS* gene in vertebrates, only mammalian *MAVS* transcripts harbor at least one uORF, highlighting a conserved and important role of uORFs in regulating mammalian MAVS function (Figure S1). The polycistronic transcript of human *MAVS* generates a full-length MAVS (MAVS-M1) from ORF1 that forms functional prion-like aggregates under stimulation, as well as an N-terminal 141-amino acid truncated isoform (MAVS-M2) from ORF2 that exerts dominant-negative effects on MAVS aggregation and its activity (Brubaker et al., 2014; Hou et al., 2011; Minassian et al., 2015; Qi et al., 2017). In addition to the main ORF1 and ORF2, human *MAVS* transcript harbors three uORFs in the 5′ UTR, named *uORF1/2/3* (Figure 1A). To study the physiological function of *MAVS* uORFs, we created vectors expressing wild-type (WT) MAVS containing the 5′ UTR (MAVS-WT) and a series of uORF-deprived mutants (MAVS-ΔuORF1/2/3/2,3/1,3/1,2/1,2,3) in *MAVS*-deficient ($Mavs^{-/-}$) HEK293T cells described previously (Shi et al., 2015). This cellular model mimicked a physiological condition because the near-endogenous expression of MAVS-WT shuts down or activates the IFN-β signaling pathway in the quiescent state or upon viral infection (Figure S2). Strikingly, expression of various MAVS mutants induced IFN-β production in the quiescent cells, and these activities were correlated with the disappearance of uORFs. When all uORFs were absent, the mutant MAVS-ΔuORF1,2,3 showed the strongest activity in stimulating IFN-β production (Figure 1B). In the absence of uORFs, other cytokines such as ISG54, interleukin (IL)-6, and CCL5 were also produced, further demonstrating that the TBK1/IRF3 and IKK/NF-κB signaling branch downstream of MAVS were activated (Figures 1C–1E). Owing to the continuous activation of IFN-β signaling pathway in the quiescent state, $Mavs^{-/-}$ cells expressing MAVS-ΔuORF1,2,3 exhibited robust antiviral activities against Sendai virus (SeV) or vesicular stomatitis virus (VSV) (Figures 1F–1H). These results indicate that deletion of *MAVS* uORFs leads to activation of the MAVS-dependent signaling pathway without viral infection.

Furthermore, we examined if the *MAVS* uORF-mediated regulation of the IFN signaling pathway exists in *Mus musculus*. To this end, mouse *MAVS*-deficient (m$Mavs^{-/-}$) MEF cells constructed previously (Hou et al., 2011) were used for ectopic expression of WT mouse MAVS (mMAVS-WT), as well as the sole uORF-deprived mutant (mMAVS-ΔuORF) (Figure 2A). Compared with mMAVS-WT, mMAVS-ΔuORF expression

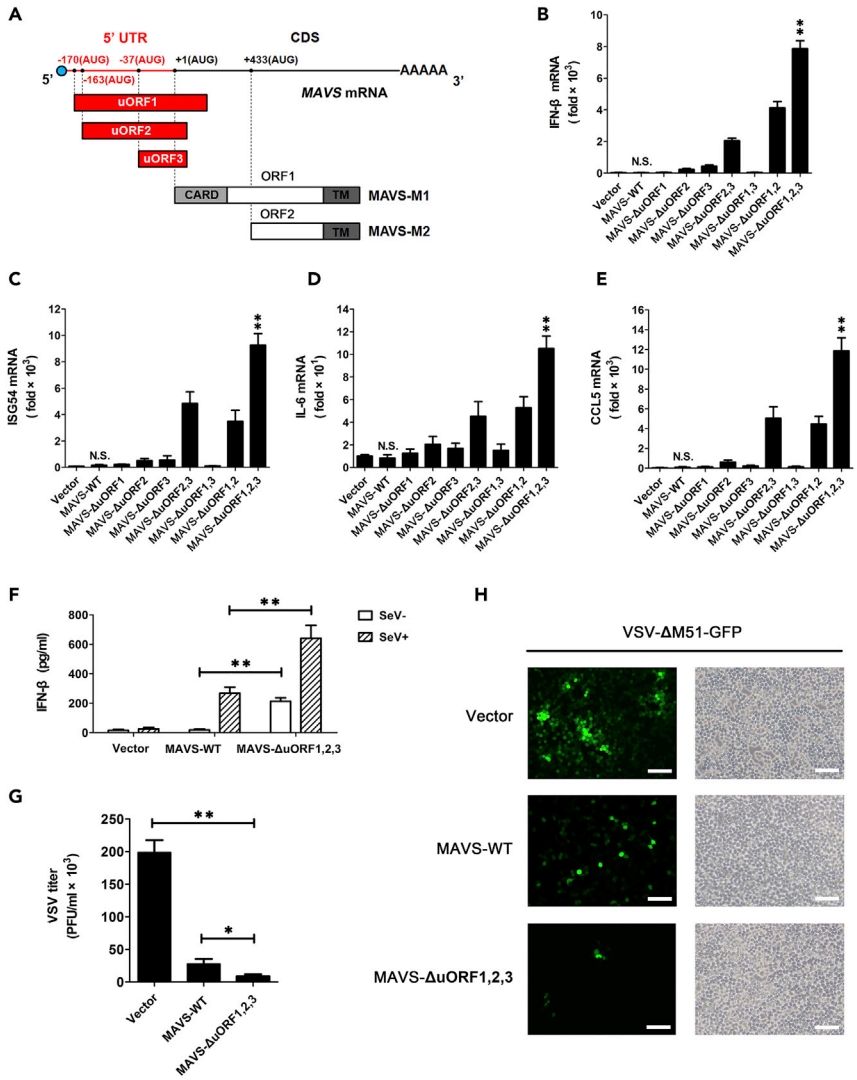

Figure 1. The MAVS-Dependent Antiviral Signaling Pathway Is Activated in the Absence of *MAVS* uORFs

(A) A diagram illustrating that three uORFs (uORF1/2/3) and two major ORFs (ORF1 and ORF2) are harbored in the 5′ UTR and coding sequence (CDS) of *MAVS* transcript, respectively.

(B–E) *Mavs*$^{-/-}$ HEK293T cells were transfected with empty vector or plasmids encoding WT MAVS with full 5′ UTR (MAVS-WT) and various uORF-deprived mutants (MAVS-ΔuORF1/2/3/2,3/1,3/1,2/1,2,3). Cells were collected 36 h post transfection. RNA was extracted and subjected to qPCR for measuring the induction of IFN-β (B), ISG54 (C), IL-6 (D), and CCL5 (E). The results show means ± SDs (n = 3, **p < 0.01, N.S., non-significant; t test).

(F) Twenty-four hours post transfection of empty vector, or plasmids encoding MAVS-WT and MAVS-ΔuORF1,2,3, *Mavs*$^{-/-}$ cells were infected with or without SeV for 12 h. ELISA was performed to measure the production of IFN-β. The results show means ± SDs (n = 3, **p < 0.01; t test).

(G and H) Transfection was performed as described in Figure 1F. Cells were infected with VSV (MOI = 1). Twelve hours post-infection, VSV titers were quantitated by plaque assay (G). Fluorescent images were taken to examine VSV proliferation 8 h after infection (H). Scale bar, 20 μm. The results show means ± SDs (n = 3, *p < 0.05, **p < 0.01; t test).

dramatically induced IFN-β production in a dose-dependent manner in m*Mavs*$^{-/-}$ MEF cells (Figure 2B). The production of cytokines IL-6 and CXCL10 was also detected when mMAVS-ΔuORF was expressed (Figures 2C and 2D). Consistent with the results in *Mavs*$^{-/-}$ HEK293T cells, infection of m*Mavs*$^{-/-}$ MEF cells with VSV enhanced the level of type I IFN that was fore-produced under expression of mMAVS-ΔuORF (Figures 2E and 2F), thereby leading to a quick clearance of virus (Figure 2G). Taken together, our data reveal that the presence of *MAVS* uORFs blocks the MAVS-mediated activation of IFN signaling pathway in the quiescent cells.

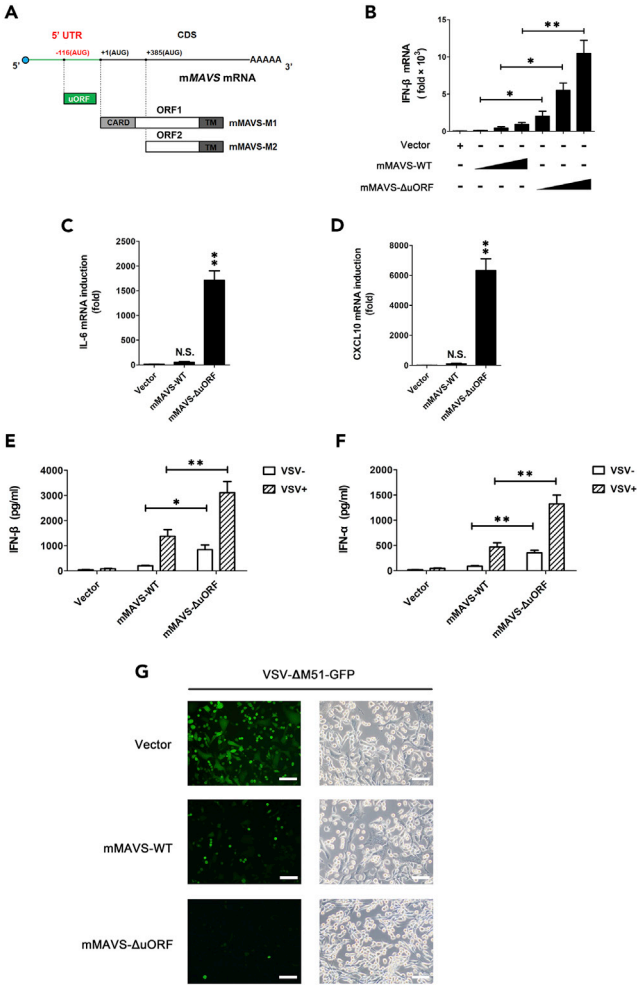

Figure 2. Expression of MAVS in the Absence of uORF Provokes an Antiviral State in *Mavs*$^{-/-}$ MEF Cells

(A) An illustrated diagram showing the position of uORF and two ORFs (ORF1 and ORF2) in the 5′ UTR and CDS of mouse *MAVS* (m*MAVS*) transcript.

(B) *Mavs*$^{-/-}$ MEF cells were transfected with empty vector or increasing doses of plasmids encoding WT mouse MAVS with full 5′ UTR (mMAVS-WT) and its mutant lacking uORF (mMAVS-ΔuORF). Cells were collected 36 h post transfection. RNA was extracted and subjected to qPCR for measuring the induction of IFN-β. The results show means ± SDs (n = 3, *p < 0.05, **p < 0.01; t test).

(C and D) Empty vector or expressing plasmids for mMAVS-WT and mMAVS-ΔuORF were transfected into *Mavs*$^{-/-}$ MEF cells. Thirty-six hours post transfection, cells were collected and RNA was extracted. qPCR was conducted for measuring the induction of IL-6 (C) and CXCL10 (D). The results show means ± SDs (n = 3, **p < 0.01, N.S., non-significant; t test).

(E and F) Transfection was performed as described in Figure 2C. Twenty-four hours post transfection, *Mavs*$^{-/-}$ MEF cells were infected with or without VSV (MOI = 1) for 12 h. ELISA was performed to measure the production of IFN-β (E) and IFN-α (F). The results show means ± SDs (n = 3, *p < 0.05, **p < 0.01; t test).

(G) Twenty-four hours post transfection of empty vector, or expressing plasmids for mMAVS-WT and mMAVS-ΔuORF, *Mavs*$^{-/-}$ MEF cells were infected with VSV (MOI = 1). Fluorescent images were taken to examine VSV proliferation 8 h post infection. Scale bar, 20 μm.

MAVS Generated from the uORF-Deprived Transcript Is Spontaneously Aggregated

Given that the prion-like filament formation of MAVS is essential for activating IFN signaling pathway, we sought to determine whether uORFs directly regulate MAVS aggregation. When endogenous *MAVS* transcription was activated by a commercial CRISPR/dCas9 system, we found that the nearly 3-fold induction of *MAVS* mRNA stimulated IFN-β production in HEK293T cells without viral infection (Figure 3A). Compared with the control group, the increased *MAVS* transcripts raised the protein level of endogenous MAVS, which formed prion-like aggregates as visualized on semidenaturing detergent agarose gel

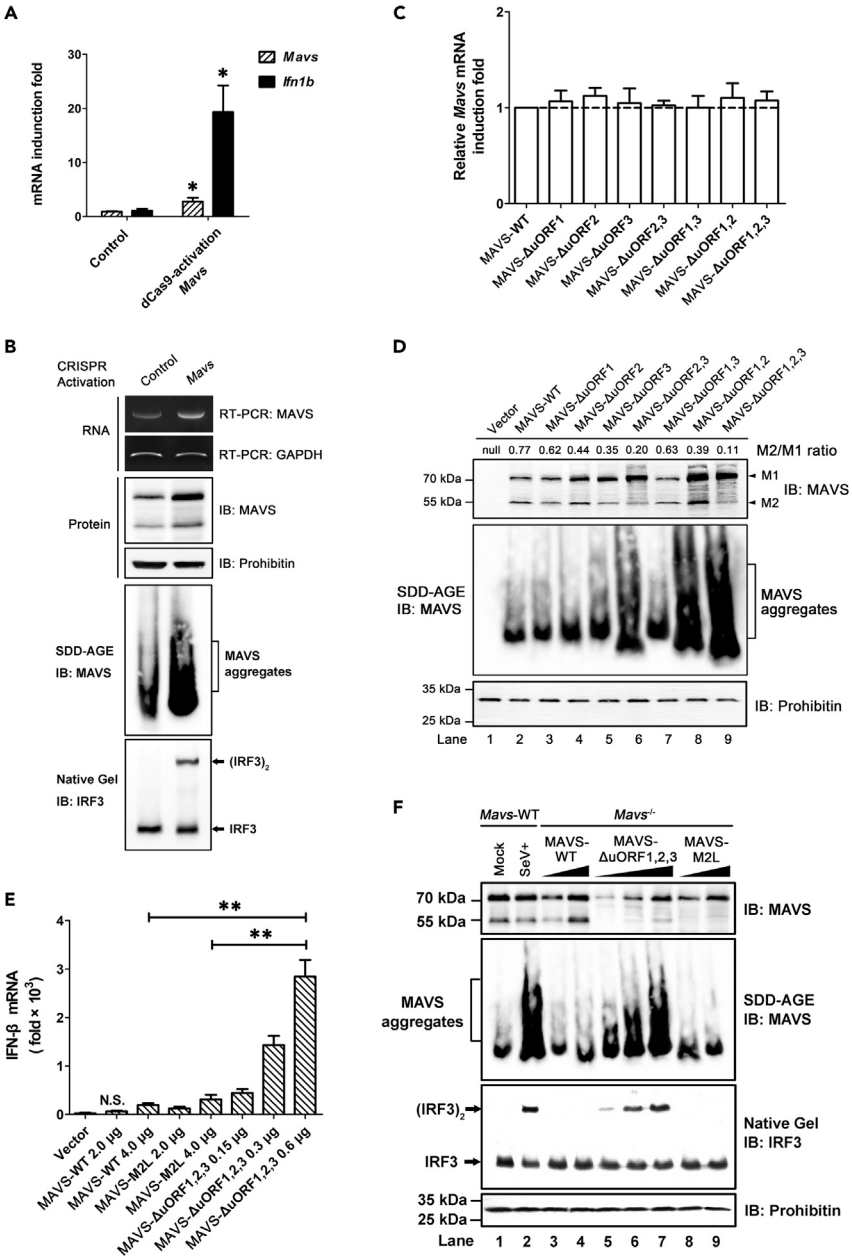

Figure 3. Absence of uORFs in the *MAVS* Transcript Leads to the Spontaneous Aggregation of MAVS

(A and B) HEK293T cells were transfected with the CRISPR/dCas9-mediated transcriptional activation plasmids targeting *MAVS* or a control plasmid. Cells were harvested 48 h post transfection. RNA was extracted and subjected to qPCR analysis for measuring the induction of *MAVS* mRNA and IFN (A). P5 fractions were isolated and used to examine MAVS aggregation and activity in inducing IRF3 dimerization *in vitro* (B). Immunoblotting (IB) was conducted for analyzing the protein level of MAVS. Mitochondrial outer membrane protein prohibitin was immunoblotted as an internal control. RT-PCR was performed to measure the mRNA level of *MAVS* gene. GAPDH was analyzed as an internal control.

(C and D) Transfection was performed as described in Figure 1B. Thirty-six hours post transfection, cells were harvested and RNA was extracted to measure the mRNA level of *MAVS* gene by qPCR analysis (C). P5 fractions were isolated and used to examine MAVS aggregation and activity in inducing IRF3 dimerization *in vitro*. Immunoblotting was conducted for analyzing the protein level of full-length MAVS M1 and isoform M2. The relative ratios of M2/M1 from each lane were quantified (D).

(E and F) Empty vector, or increasing doses of plasmids encoding MAVS-WT, MAVS-M2L, and MAVS-ΔuORF1,2,3 were transfected into *Mavs*$^{-/-}$ HEK293T cells. Thirty-six hours post transfection, cells were harvested and RNA was extracted to measure the IFN induction by qPCR analysis (E). P5 fractions were isolated and used to examine MAVS aggregation and

Figure 3. *Continued*
activity in inducing IRF3 dimerization *in vitro* (F). Immunoblotting was conducted for analyzing the protein level of MAVS. P5 fractions from SeV-infected HEK293T cells were analyzed as positive control. The results show means ± SDs (n = 3, **p < 0.01, N.S., non-significant; t test).

electrophoresis (SDD-AGE) and was able to stimulate IRF3 dimerization in a cell-free system (Zeng et al., 2009) (Figure 3B). To see if uORFs regulate MAVS aggregation in this manner, vectors encoding MAVS-WT and various uORF-deprived mutants were introduced into *Mavs*$^{-/-}$ HEK293T cells. Although deleting uORFs had no impacts on the mRNA level, the uORF-deprived MAVS transcripts generated more functional M1 proteins and attenuated the production of the negative isoform M2, thus leading to a drop in the M2/M1 ratio at the protein level (Figures 3C and 3D). It was suggested that uORF1 and uORF2 collaborate to repress M1 translation (Figure 3D, compare lanes 2, 4, and 8), whereas uORF3 facilitates M2 translation (Figure 3D, compare lanes 2 and 5; compare lanes 8 and 9). Notably, deletion of uORFs caused dramatic accumulation of the functional M1 protein along with elimination of the negative isoform M2, thus resulting in MAVS spontaneous aggregation as visualized on SDD-AGE (Figure 3D, lanes 6, 8, and 9). These data suggest that deletion of uORFs promotes MAVS to spontaneously aggregate by reducing the M2/M1 ratio rather than by enhancing MAVS transcription.

If the low M2/M1 ratio was a prerequisite for the spontaneous aggregation of MAVS, then we would expect that MAVS spontaneously aggregates when M2 is completely eliminated. However, when a high dosage of vector expressing the MAVS mutant lacking M2 (MAVS-M2L) was introduced into *Mavs*$^{-/-}$ cells, neither MAVS aggregates nor IFN-β mRNA induction was detected in the absence of the negative isoform M2 (Figures 3E and 3F, lane 9). In contrast, although we detected M2 expression in the absence of uORFs, the below-physiological protein level of M1 was able to promote MAVS spontaneous aggregation. The nature and activity of spontaneously aggregated MAVS were the same as those of SeV-stimulated MAVS, thereby stimulating IRF3 dimerization and IFN-β production (Figures 3E and 3F, compare lanes 2 and lanes 5–7). In conclusion, we uncover that MAVS generated from the uORF-deprived transcript is qualified to spontaneously aggregate and activate the IFN signaling pathway without viral infection.

uORFs Are *Cis*-Acting Elements that Repress MAVS Translation by Leaky Scanning

The above data all pointed to a regulatory role of uORFs in *MAVS* downstream ORF translation. Next, we addressed whether uORFs function as *trans*-factors or *cis*-elements. For this purpose, MAVS-WT, MAVS-ΔuORF1,2,3, or MAVS-ΔuORF1,2,3 along with vectors expressing uORF1, 2, and 3 were introduced into *Mavs*$^{-/-}$ cells. To enhance the translation efficiency and the stability of putative short peptides encoded by uORFs, FLAG tag and GFP were fused to the N and C termini of uORFs. If *MAVS* uORFs were *trans*-factors repressing downstream ORF translation, then we would expect that recovery of uORF-encoded peptides in the absence of uORFs can block MAVS translation and its spontaneous aggregation, thereby returning the IFN-β mRNA to the physiological level. When uORFs are absent, however, recovery of Flag-uORF1/2/3, uORF1/2/3-GFP, or uORF1,2,3 failed to block the IFN-β production stimulated by spontaneously aggregated MAVS, demonstrating that uORFs do not act in *trans* (Figure 4A). Subsequently, we tested the hypothesis that uORFs function as *cis*-acting elements. Among these uORFs, uORF2 is the dominant inhibitory element that blocks MAVS translation, because deleting uORF1 and 3 cannot remove the dominant-negative effects on IFN-β mRNA induction (Figure 4B, see MAVS-uORF2). Nevertheless, additionally deleting uORF2 on the basis of MAVS-ΔuORF1 and 3 completely accelerated MAVS translation, thereby leading to IFN-β stimulation (Figure 4B, see MAVS-ΔuORF1,2,3). We generated a specific antibody against the putative short peptide encoded by uORF2, but failed to detect its expression in HEK293T cells by immunoblotting (Figure S3A). All these data show that *MAVS* uORFs act in *cis* to repress downstream ORF translation.

Typically, the cap-dependent ribosome scanning initiates protein translation at the first optimal start codon in eukaryotes (Kozak, 1999). Two uncanonical mechanisms, reinitiation and leaky scanning, are usually employed by uORFs to downregulate their associated downstream coding ORF (Kozak, 1986, 1987). The reinitiation mechanism accounts for the observation that 40S ribosomal subunits resume to scan and initiate at a downstream AUG codon after translating a small independent uORF. Leaky scanning occurs when 40S subunits ignore the initial start codon with a less than strong or optimal context, which is known as the *Kozak sequence* (GCC^{A}/$_{G}$CCAUGG), and continue scanning along the mRNA to initiate at a downstream AUG codon (Kozak, 2002). Given that *MAVS* uORF2 overlaps with the start codon of downstream ORF1 and functions as the dominant inhibitory element, we hypothesized that full-length MAVS

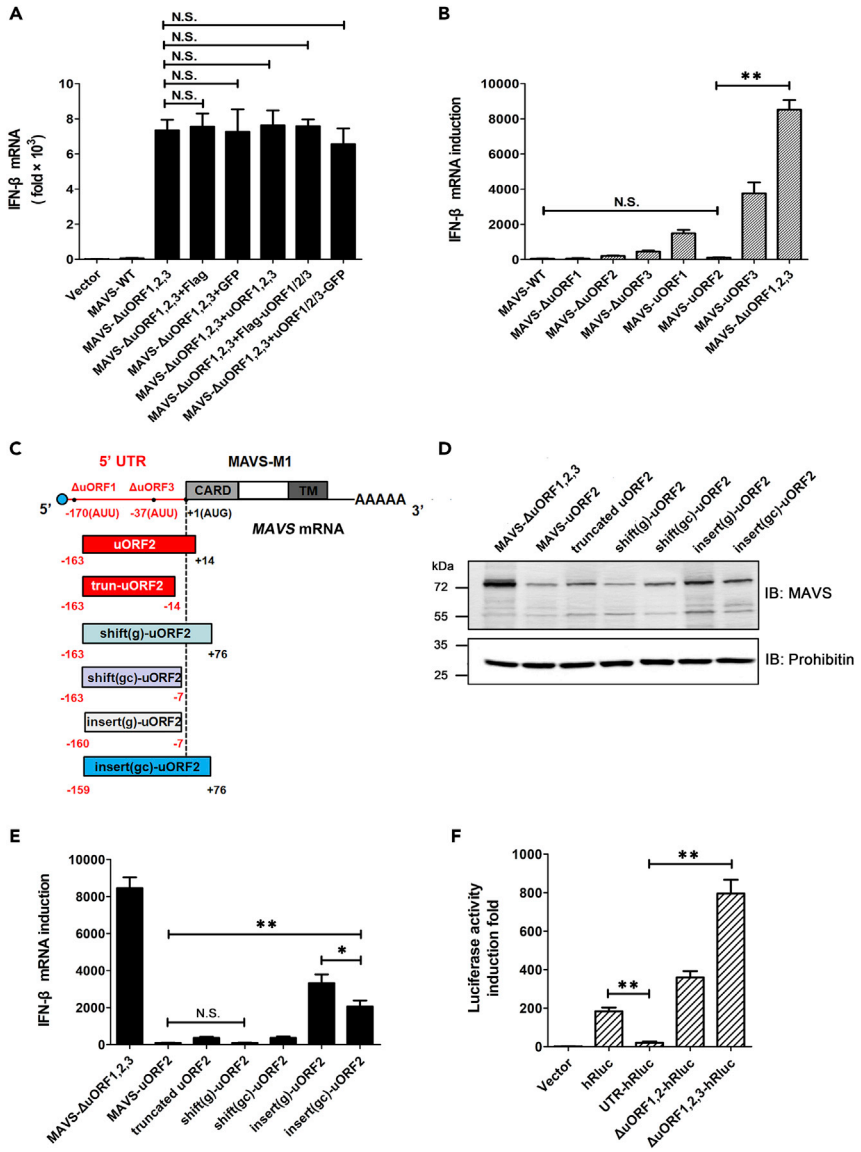

Figure 4. uORFs Exerts *cis*-Acting Repression of MAVS Translation

(A) Plasmid encoding MAVS-ΔuORF1,2,3 were co-transfected into *Mavs*$^{-/-}$HEK293T cells with indicated expression vectors. Empty vector and plasmid encoding MAVS-WT were transfected as control. Cells were harvested 36 h post transfection. RNA was extracted and subjected to qPCR analysis for measuring the induction of IFN. The results show means ± SDs (n = 3, t test).

(B) *Mavs*$^{-/-}$ HEK293T cells were transfected with expression vectors for MAVS-WT and various uORF-deprived mutants as indicated. Thirty-six hours post transfection, cells were harvested and RNA was extracted to measure the induction of IFN by qPCR analysis. The results show means ± SDs (n = 3, **p < 0.01, N.S., non-significant; t test).

(C) A diagram showing the WT and a series of artificial *MAVS* uORF2. Positions of AUG codons and stop codons are indicated. See also Table S1.

(D and E) Plasmids encoding MAVS-ΔuORF1,2,3, MAVS-uORF2, and various artificial MAVS-uORF2 were transfected into *Mavs*$^{-/-}$ HEK293T cells. Cells were harvested 36 h post transfection. P5 fractions were isolated and used to analyze the protein level of MAVS by immunoblotting (D). RNA was extracted to measure the induction of IFN by qPCR analysis (E). See also Figure S3B. The results show means ± SDs (n = 3, *p < 0.05, **p < 0.01, N.S., non-significant; t test).

(F) HEK293T cells were transfected with empty vector, or expression vectors for hRluc, UTR-hRluc, ΔuORF1,2-hRluc, and ΔuORF1,2,3-hRluc. Thirty-six hours post transfection, cell lysates were collected for measuring the luciferase activities. The results show means ± SDs (n = 3, **p < 0.01; t test).

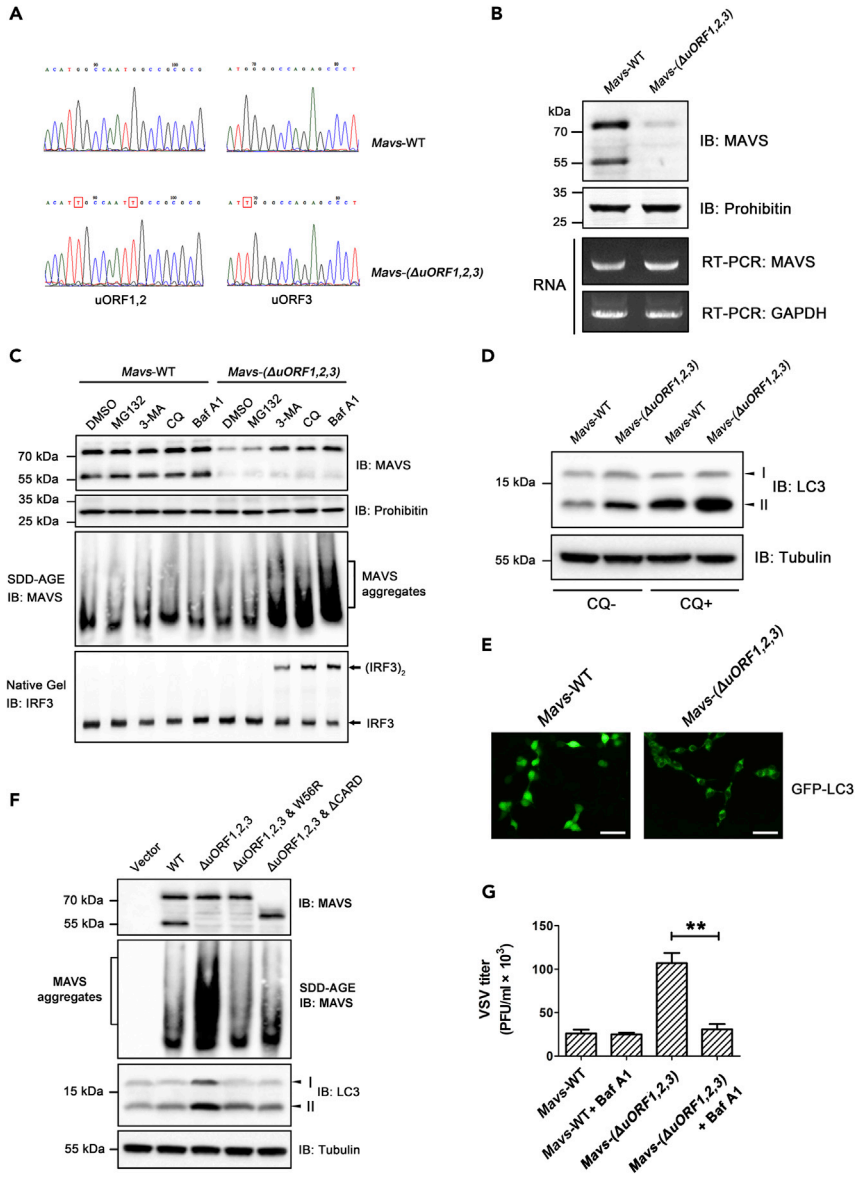

Figure 5. Spontaneously Aggregated MAVS in *Mavs-(ΔuORF1,2,3)* Cells Is Degraded through the Autophagy Pathway

(A) Sequencing of uORFs in the *MAVS* gene from WT and *Mavs-(ΔuORF1,2,3)* HEK293T cells. ATG start codons of uORFs in the *MAVS* genomic sequence were replaced with ATT by CRISPR/Cas9-mediated knockin. See also Figure S4A.

(B) P5 fractions of WT and *Mavs-(ΔuORF1,2,3)* HEK293T cells were obtained to determine endogenous MAVS protein level by immunoblotting (IB). Prohibitin was immunoblotted as a loading control. RT-PCR was performed to measure mRNA level of the *MAVS* gene. GAPDH was analyzed as an internal control.

(C) WT and *Mavs-(ΔuORF1,2,3)* HEK293T cells were treated with MG132 (10 μM), 3-methyladenine (3-MA) (10 mM), chloroquine (CQ) (30 μM), or bafilomycin A1 (Baf A1) (0.2 μM) for 4 h. P5 fractions were obtained and used to examine MAVS aggregation and activity in inducing IRF3 dimerization *in vitro*. Immunoblotting was conducted for analyzing the protein level of MAVS.

(D) WT and *Mavs-(ΔuORF1,2,3)* HEK293T cells were treated with or without 30 μM CQ for 4 h. Whole-cell lysates were subjected to immunoblotting for analyzing the protein level of LC3-I and LC3-II. Tubulin was immunoblotted as a loading control.

(E) WT and *Mavs-(ΔuORF1,2,3)* HEK293T cells were transfected with plasmid encoding GFP-tagged LC3 (GFP-LC3). Fluorescent images were taken at 36 h post transfection. Scale bar, 20 μm. See also Figure S4B.

(F) *Mavs*$^{-/-}$ HEK293T cells were transfected with empty vector, or expression plasmids for MAVS-WT, MAVS-ΔuORF1,2,3, MAVS-ΔuORF1,2,3 & W56R, and MAVS-ΔuORF1,2,3 & ΔCARD. Cells were harvested at 36 h post transfection. P5 fractions

Figure 5. *Continued*
were obtained and used to examine MAVS aggregation. Whole-cell lysates were subjected to immunoblotting for analyzing the protein level of LC3-I and LC3-II.
(G) WT and *Mavs-(ΔuORF1,2,3)* HEK293T cells were treated with or without 0.2 μM Baf A1 for 4 h. Cells were infected with VSV (MOI = 1) for 12 h and then subjected to the plaque assay for quantitating VSV titers. The results show means ± SDs (n = 3, **p < 0.01; t test).

is translated under the regulation of uORF2 by leaky scanning. To test this hypothesis, we constructed a series of vectors based on MAVS-uORF2 to truncate uORF2, shift the frame of uORF2, and weaken the initiation efficiency of uORF2 AUG codon by changing the translation context from suboptimal to weak (Figure 4C and Table S1). These artificial uORF2 mutants were expressed in *Mavs*$^{-/-}$ cells to determine MAVS translation and IFN-β mRNA induction, by comparison with the IFN-β-stimulating mutant MAVS-ΔuORF1,2,3 and the IFN-β-blocking mutant MAVS-uORF2.

Consistent with the observations from the gain-of-function experiment conducted in Figure 4A, shifting the frame of uORF2 cannot remove the dominant-negative effects on MAVS-M1 translation and IFN-β stimulation, further demonstrating that the *cis*-acting manner of uORF2 is independent on its coded short peptide (Figures 4D and 4E, compare shift(g)-uORF2 and MAVS-uORF2). Notably, artificial uORF2 start codon with a weak translational context was leaky and facilitated ribosomes to proceed and more efficiently translate MAVS-M1, thereby leading to a dramatic induction in IFN-β mRNA (Figures 4D and 4E, compare insert(gc)-uORF2 and MAVS-uORF2). In addition, truncating or shifting the reading frame caused early termination of uORF2 before the ORF1 start site, allowing ribosomes to resume scanning and reinitiate at the ORF1 start codon. As a result, the translation of MAVS-M1 and IFN-β stimulation is more efficient when reinitiation and leaky scanning simultaneously occur (Figures 4D and 4E, compare insert(g)-uORF2 and insert(gc)-uORF2). These modifications did not impair the stability and amounts of *MAVS* transcripts (Figure S3B). Furthermore, *MAVS* uORFs downregulated the translation of heterologous genes such as Renilla luciferase (hRluc), highlighting the potential of *MAVS* uORFs as a general *cis*-regulatory element for broad repression of downstream ORF translation (Figure 4F). Overall, our data reveal that uORFs exert *cis*-acting repression of the full-length MAVS translation by leaky scanning.

Absence of uORFs Results in the Endogenous MAVS Degradation

To further uncover the physiological significance of *MAVS* uORFs, we generated a HEK293T cell line lacking uORFs in the endogenous *MAVS* gene by CRISPR/Cas9-mediated knockin, named as *Mavs-(ΔuORF1,2,3)*. Details can be found in Table S2 and Transparent Methods. In the genomic sequence of *MAVS*, the ATG start codons were replaced with ATT so that ribosomes did not initiate uORFs translation (Figure 5A). We further performed 5′ rapid amplification of cDNA ends analysis of the *MAVS* transcripts in *Mavs-(ΔuORF1,2,3)* cells and showed that the start codons of *MAVS* uORFs in the 5′-UTR have already been changed (Figure S4A). Given the elimination of translational blockage from uORFs, endogenous MAVS was expected to more efficiently express. To our surprise, endogenous MAVS protein from the allele that was devoid of uORFs, MAVS-(ΔuORF1,2,3), was expressed at an extremely lower level in contrast to that from *Mavs*-WT cells (Figure 5B). Low protein level of MAVS-(ΔuORF1,2,3) was not due to transcriptional difference, because comparable amounts of mRNAs were detected in both mutant allele and WT cells. An explanation is that MAVS-(ΔuORF1,2,3) is degraded once uORFs in the 5′-UTR are absent. Thus, we were interested in seeking the way by which endogenous MAVS protein is degraded in *Mavs-(ΔuORF1,2,3)* cells.

Autophagy Is Responsible for Degradation of the Spontaneously Aggregated MAVS

The ubiquitin-proteasome system and the autophagy process are two major protein degradation pathways required for maintaining cellular homeostasis. To determine which pathway might be responsible for degradation of MAVS-(ΔuORF1,2,3), we treated *Mavs-(ΔuORF1,2,3)* and WT cells with proteasome and autophagy inhibitors. Treatment with autophagy inhibitor 3-methyladenine or autolysosome inhibitors chloroquine (CQ) and bafilomycin A1 (Baf A1), but not proteasome inhibitor MG132, resulted in dramatical accumulation of MAVS-(ΔuORF1,2,3), suggesting that the autophagic-lysosomal pathway is responsible for MAVS-(ΔuORF1,2,3) degradation (Figure 5C, upper panel). It was noticed that the accumulated MAVS-(ΔuORF1,2,3) was spontaneously aggregated and capable of activating IRF3, as the formation of prion-like aggregates and IRF3 dimerization was detected under treatment with autophagy inhibitors (Figure 5C, lower panel). In general, the conversion of the soluble form of LC3 (LC3-I) to the phosphatidylethanolamine-bound LC3 form (LC3-II) has been widely

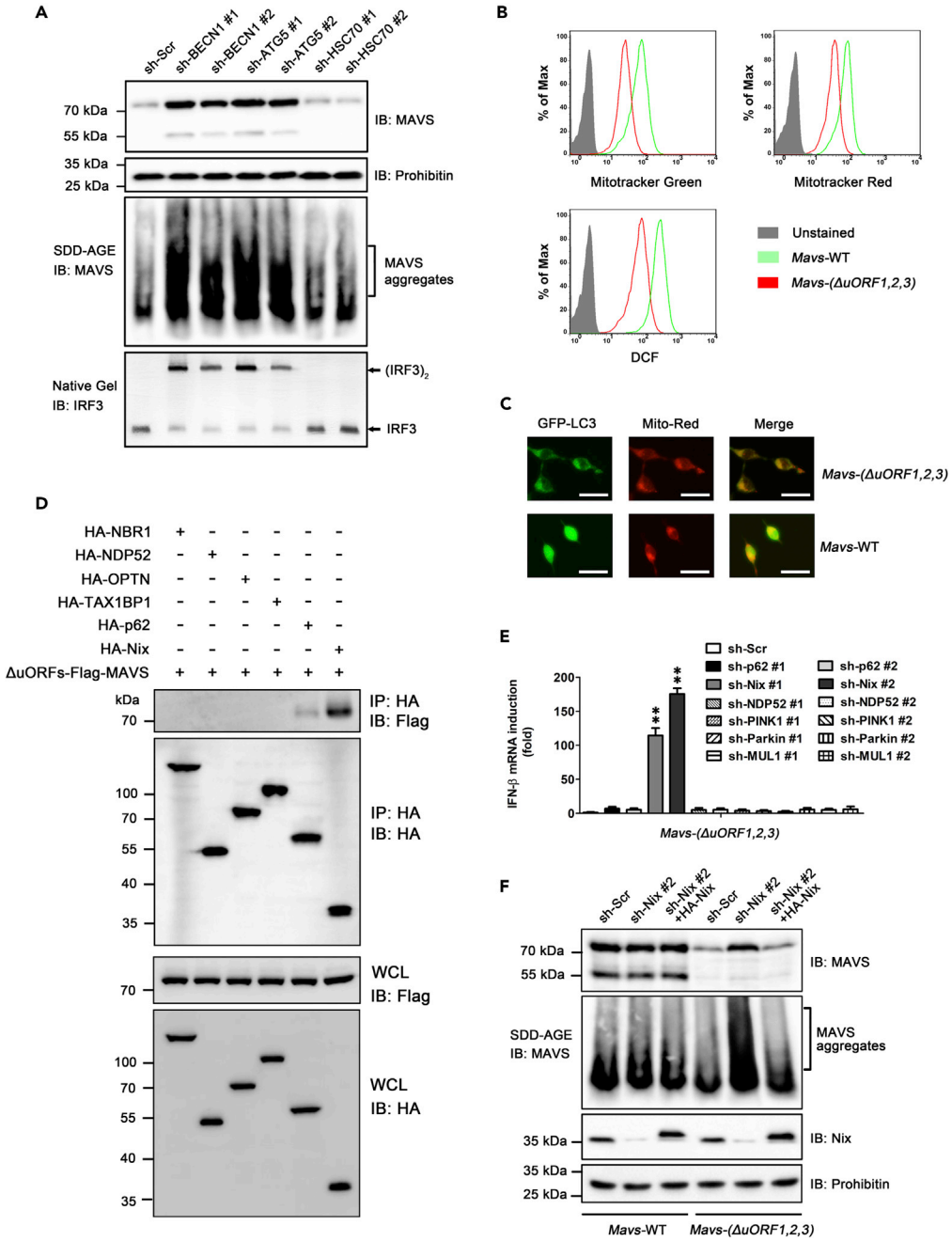

Figure 6. Nix-Mediated Mitophagy Is Responsible for Elimination of Spontaneously Aggregated MAVS in *Mavs-(ΔuORF1,2,3)* Cells

(A) *Mavs-(ΔuORF1,2,3)* HEK293T cells were transfected with constructs expressing scramble short hairpin RNA (shRNA) (sh-Scr), sh-Beclin 1 (BECN1) (#1 and #2), sh-ATG5 (#1 and #2), or sh-HSC70 (#1 and #2). After 36 h, second transfection was performed. Cells were collected 36 h post the second transfection. P5 fractions were isolated to examine MAVS aggregation and activity in inducing IRF3 dimerization *in vitro*. See also Figure S5A.

(B) Fluorescence-activated cell sorting (FACS) analysis showing that mitophagy clears up damaged mitochondria and diminishes ROS production in *Mavs-(ΔuORF1,2,3)* cells. WT and *Mavs-(ΔuORF1,2,3)* cells were stained with 200 nM MitoTracker Green (which stains the lipid membrane of total mitochondria) and 150 nM MitoTracker Red (which fluoresces upon oxidation in respiring mitochondria). For determination of mitochondrial ROS production, cells were stained with 2 μM DCFH-DA (2,7-Dichlorodi-hydrofluorescein diacetate, which would be transformed to fluorescent compound DCF by ROS). After 20 min of incubation, cells were collected for FACS analysis. Histograms of FACS analysis are depicted.

Figure 6. *Continued*

(C) WT and *Mavs-(ΔuORF1,2,3)* HEK293T cells were transfected with GFP-LC3 expression plasmid. Thirty-six hours post transfection, cells were stained with 150 nM MitoTracker Red (Mito-Red) and incubated for 20 min before taking the fluorescent images. Scale bar, 20 μm.

(D) pcDNA-ΔuORFs-Flag-MAVS was transfected into *Mavs*$^{-/-}$ HEK293T cells together with plasmids encoding various hemagglutinin (HA)-tagged autophagy cargo receptors as indicated. Thirty-six hours post transfection, cells were collected and subjected to immunoprecipitation and immunoblotting.

(E) Constructs encoding shRNAs targeting various cargo receptors and mitophagy-related genes were transfected into *Mavs-(ΔuORF1,2,3)* cells, as described in Figure 6A. RNA was extracted from collected cells, and qPCR was performed to measure IFN induction. The results show means ± SDs (n = 3; **p < 0.01; t test). See also Figure S6A.

(F) WT and *Mavs-(ΔuORF1,2,3)* HEK293T cells were transfected with sh-Scr, sh-Nix, or together with the rescue vector HA-Nix. Cells were collected at 36 h post transfection. P5 fractions were isolated to examine MAVS aggregation. Immunoblotting was conducted to analyze the protein level using anti-MAVS and anti-Nix antibodies.

used as indicators of autophagic activity (Klionsky et al., 2008). Compared with *Mavs*-WT cells, LC3-II level was much higher in *Mavs-(ΔuORF1,2,3)* cells with or without CQ treatment, suggesting that the accumulation of LC3-II in *Mavs-(ΔuORF1,2,3)* cells was due to robust autophagic activity (Figure 5D). Consistently, GFP-LC3 puncta was observed in *Mavs-(ΔuORF1,2,3)* cells, but not in *Mavs*-WT cells (Figures 5E and S4B). These results together demonstrate that the autophagy pathway is continuously activated in *Mavs-(ΔuORF1,2,3)* cells.

Given the blockage of autophagy pathway accumulated endogenous MAVS-(ΔuORF1,2,3) that is spontaneously aggregated, we next addressed if the aggregation of MAVS-(ΔuORF1,2,3) could induce autophagy. For this purpose, MAVS-WT and MAVS-ΔuORF1,2,3 were expressed in *Mavs*$^{-/-}$cells to examine MAVS aggregation and LC3-II accumulation. In addition, we introduced the point mutation W56R into MAVS-ΔuORF1,2,3, which was reported to prevent MAVS filament formation (Wu et al., 2014), and deleted the CARD domain that is essential for aggregation (Hou et al., 2011). The prion-like aggregates, as well as high level of LC3-I and LC3-II, were detected in *Mavs*$^{-/-}$cells expressing MAVS-ΔuORF1,2,3, but not MAVS-WT, MAVS-ΔuORF1,2,3 & W56R, or MAVS-ΔuORF1,2,3 & ΔCARD (Figure 5F), confirming our speculation that the continuously activated autophagy in *Mavs-(ΔuORF1,2,3)* cells was induced by the spontaneously aggregated MAVS-(ΔuORF1,2,3). Furthermore, we found that loss of MAVS-(ΔuORF1,2,3) resulted in compromised IFN production and antiviral effects on viral proliferation in *Mavs-(ΔuORF1,2,3)* cells upon VSV infection, whereas blockage of autophagy by Baf A1 accumulated MAVS-(ΔuORF1,2,3) and restored its antiviral activities (Figures 5G and S4C). Altogether, our findings indicate that the spontaneously aggregated MAVS-(ΔuORF1,2,3) triggers autophagy and is subjected to autophagic degradation.

Cargo Receptor Nix Is Required for the Mitophagic Degradation of Spontaneously Aggregated MAVS

There are three types of autophagy: chaperone-mediated autophagy (CMA), microautophagy, and macroautophagy (hereafter referred to as autophagy). To determine which pathway is indeed responsible for degradation of spontaneously aggregated MAVS-(ΔuORF1,2,3), we knocked down the expression of two essential components in macroautophagy, Beclin-1 (BECN1) and ATG5 (Liang et al., 1999; Mizushima et al., 1998), as well as the CMA chaperone protein HSC70, which captures and drives the target proteins to lysosomes (Agarraberes et al., 1997). Treatment with either sh-BECN1 or sh-ATG5, but not sh-HSC70, led to marked accumulation of MAVS-(ΔuORF1,2,3) in *Mavs-(ΔuORF1,2,3)* cells (Figures 6A, upper panel and S5A). As expected, the accumulated MAVS-(ΔuORF1,2,3) was spontaneously aggregated and capable of activating the IFN signaling pathway (Figures 6A, lower panel and S5B). In contrast, these phenomena were not observed in *Mavs*-WT cells. We thus concluded that the degradation of spontaneously aggregated MAVS-(ΔuORF1,2,3) is independent of CMA.

Mitochondrial autophagy (mitophagy) is a specific autophagic pathway by which damaged mitochondria are selectively targeted for degradation (Randow and Youle, 2014). As the spontaneously aggregated MAVS-(ΔuORF1,2,3) is located in the mitochondria and induces continuous activation of autophagy, we hypothesized that mitophagy is responsible for the selective degradation of MAVS-(ΔuORF1,2,3). As a result of the mitophagic clearance, both total mitochondria (stained with MitoTracker Green) and healthy mitochondria (stained with MitoTracker Red) were remarkably reduced, thereby resulting in compromised reactive oxygen species (ROS) production in *Mavs-(ΔuORF1,2,3)* cells (Figure 6B). The colocalization of GFP-LC3 puncta with mitochondria in *Mavs-(ΔuORF1,2,3)* cells also indicated the initiation of mitophagy (Figure 6C). In addition to MAVS, other mitochondrial outer membrane proteins like Bcl-2 and VDAC1

diminished along with the disappearance of total mitochondria, further demonstrating that mitophagy was provoked in the absence of *MAVS* uORFs (Figure S5C). Indeed, expression of MAVS-ΔuORF1,2,3 enhanced ROS production and induced mitophagy, whereas introducing W56R, ΔCARD, or ΔTM mutation into MAVS-ΔuORF1,2,3 abolished its capabilities of inducing mitophagy, indicating that MAVS aggregation and its mitochondrial location are required for inducing mitophagy (Figure S5D). These collective findings suggest that mitophagy is induced by the spontaneously aggregated MAVS to eliminate damaged mitochondria and MAVS aggregates in the absence of *MAVS* uORFs.

Increasing evidence shows that substrates are recognized by cargo receptors and delivered to the autophagosome for selective degradation (Boyle and Randow, 2013; Shibutani et al., 2015). We next determined which cargo receptor is essential for the recognition and mitophagic degradation of MAVS-(ΔuORF1,2,3). Coimmunopreciptation detected the interaction of MAVS-ΔuORF1,2,3 with cargo receptor p62 and Nix, but not NBR1, NDP52, Optineurin (OPTN), or TAX1BP1 (Figure 6D). To further confirm that endogenous MAVS-(ΔuORF1,2,3) is indeed degraded by p62- or Nix-mediated mitophagy that is independent of the PINK1/Parkin/MUL1 pathway, the expression of p62, Nix, PINK1, Parkin, and MUL1, as well as NDP52, which was reported to mediate ubiquitin-dependent autophagic degradation of MAVS (Jin et al., 2017), were knocked down in *Mavs-(ΔuORF1,2,3)* cells (Figure S6A). Obviously, knockdown of Nix induced IFN-β production and accumulated MAVS-(ΔuORF1,2,3) that was spontaneously aggregated (Figures 6E and 6F). This phenotype can be rescued by ectopically expressing Nix in sh-Nix-treated cells, confirming that Nix-mediated mitophagy is responsible for degradation of MAVS-(ΔuORF1,2,3). Moreover, we found that the recognition of MAVS-(ΔuORF1,2,3) by Nix is dependent on MAVS aggregation and its mitochondrial location, as introduction of W56R, ΔCARD, or ΔTM mutation into MAVS-ΔuORF1,2,3 completely blocked its interaction with Nix (Figure S6B). These results suggest that the spontaneously aggregated MAVS-(ΔuORF1,2,3) is recognized by cargo receptor Nix and subjected to mitophagic degradation.

DISCUSSION

Regulation of innate immune signaling pathway is critical for cellular response to virus infection, as well as maintenance of homeostasis in the quiescent state. As an adaptor protein, MAVS is under strict regulation for not only keeping it ready for transducing the antiviral signaling but also forestalling MAVS spontaneous aggregation, which would result in detrimental inflammation and autoimmune diseases like SLE (Buskiewicz et al., 2016; Shao et al., 2016). Our previous studies uncovered two post-translational regulation mechanisms by which MAVS is kept from spontaneous aggregation in the quiescent cells. (1) An autoinhibitory mechanism (intramolecular level). The functional domains of MAVS activating IRF3 and NF-κB are sequestered and inhibited by their adjacent regions (Shi et al., 2015). (2) The polycistronic mRNA strategy (intermolecular level). Multiple truncated isoforms generated from the polycistronic transcript interact with the full-length MAVS and block its aggregation (Qi et al., 2017). In this work, we reveal a post-transcriptional regulation that prevents MAVS spontaneous aggregation. uORFs in the *MAVS* transcript serve as "safety checks" for the quality control of MAVS translation, thereby preventing MAVS spontaneous aggregation and avoiding the accidental activation of IFN signaling pathway in the quiescent cells. Our collective findings explore the uORF physiological role in maintaining cellular homeostasis and provide a complete picture describing MAVS self-regulation at multi-levels.

In our study, the uORF-mediated regulation of MAVS is characterized by the following features. First, *MAVS* uORFs are *cis*-acting elements rather than *trans*-acting factors. Collective results from the gain-of-function experiment and shift-frame mutations rule out the possibility that uORFs control MAVS translation in *trans*. The failure of detecting *MAVS* uORFs-encoded functional peptides in cells is consistent with a previous report, by showing that the large majority of uORFs do not appear to be under selective pressure to maintain their encoded peptides (Johnstone et al., 2016). Second, *MAVS* uORF translation is more efficient than that of full-length MAVS. This is because the translational context of uORF AUG codons is suboptimal, whereas nucleotides surrounding the full-length MAVS start codon do not fit the definition of a Kozak sequence. As a result, the AUG codon with weak context is regarded as the "second choice" by ribosomal 40S subunits, which initiate leaky scanning to repress full-length MAVS translation. It should be noted, however, that we cannot exclude the possibility that reinitiation also occurs. Third, *MAVS* uORFs serve as a triple lock controlling downstream ORF translation. This regulation system is composed of three uORFs, uORF1, uORF2, and uORF3, which perform their own functions and collaborate to balance the protein production from downstream ORF1 and ORF2. Mutations analysis suggests that the production of full-length MAVS or M1 translated from ORF1 is largely controlled by uORF1 and uORF2, whereas uORF3 facilitates

the translation of ORF2. One explanation is that the cap-dependent ribosome scanning gives priority for initiation at uORF1 and uORF2 AUG codons, which are more close to the mRNA 5′ cap than that of uORF3. The translation efficiency of diverse uORFs is positively correlated with the incidence of leaky scanning, by which ribosomes can balance the translation of downstream ORF1 and ORF2. Fourth, *MAVS* uORFs can exert inhibitory impacts on endogenous gene translation. Altogether, these features establish *MAVS* uORFs as an ideal model for studying the uORF-mediated repression of downstream ORF translation and highlight the potential of *MAVS* uORFs as a general *cis*-regulatory element.

Numerous studies have noticed that ectopic expression of MAVS induces MAVS aggregation in the quiescent cell without infection. In the present work, we provide evidence that the enhanced production of endogenous MAVS via transcriptional activation can trigger its spontaneous aggregation, which strongly supports the notion that the nucleation of aggregates relies on protein concentration (Philo and Arakawa, 2009). In the *MAVS*-deficient cell model, however, MAVS-ΔuORF1,2,3 can also spontaneously aggregate even as it is ectopically expressed at a near-endogenous level. In contrast, the same protein production and expression condition cannot induce aggregation of MAVS-WT or MAVS-M2L, which lacks the dominant-negative isoform M2. More importantly, deletion of uORFs in *MAVS* gene leads to the spontaneous aggregation of endogenous MAVS. Therefore, uORFs are crucial for both quantity and quality control of MAVS. We speculate that MAVS proteins translated from the uORF-deprived transcript are out of control and converted into the nucleation foci, which serve as prion-like "seeds" for the self-perpetuating growth of aggregates. As MAVS spontaneous aggregation was reported to be associated with SLE, it is of great interest to detect *MAVS* uORF polymorphism in the genome of patients with SLE, which would establish uORF polymorphism as a molecular marker for genetic diagnosis in the future. Once *MAVS* uORFs are deficient and lose their quality control of MAVS molecules, selective autophagy of mitochondria or mitophagy is in charge of degrading MAVS aggregates. On mitochondria, spontaneously aggregated MAVS-(ΔuORF1,2,3) is suggested as a signal recognized by the cargo receptor Nix, which mediates ubiquitin-independent mitophagic degradation of MAVS aggregates. Therefore, mitophagy is an emergency response mechanism of preventing MAVS spontaneous aggregation in the quiescent cells, through the rapid clearance of MAVS aggregates.

Aberrant protein aggregation is a common theme in neurodegenerative diseases and a result of erroneous protein synthesis. For example, Alzheimer disease is strongly associated with aggregation of amyloid β-protein (Aβ) into oligomers and fibrils. Given that uORFs are prevalent across vertebrate genomes and associated with widespread translational repression, it is worth to determine whether the uORF-mediated quality and quantity control is a general mechanism of preventing abnormal protein aggregation relevant to Alzheimer, Huntington, and prion diseases. Interestingly, the polymerization is a hallmark of adaptor proteins, such as STING, MyD88, and ASC, in diverse innate immune pathways; our findings thus shed light on the regulatory roles of their uORFs in signal transduction.

Limitations of the Study

In this study, we employed an *in vitro* cellular model to demonstrate that *MAVS* undergoes uORF-mediated quantity and quality control after its transcription. To uncover the physiological significance of *MAVS* uORF-mediated regulation, further works on generating a uORF-lacking mouse model are substantially in need. It would be expected that the $Mavs^{uORFs-/-}$ mice show some symptoms of chronic inflammation and spontaneously develop SLE.

METHODS

All methods can be found in the accompanying Transparent Methods supplemental file.

Lead Contact

Dr. Nan Qi (qinan@zjut.edu.cn).

Resource and Materials Availability

Materials are available from the corresponding author on reasonable request.

DATA AND CODE AVAILABILITY

All data is available in the main text or the Supplemental Information.

SUPPLEMENTAL INFORMATION

Supplemental Information can be found online at https://doi.org/10.1016/j.isci.2020.101059.

ACKNOWLEDGMENTS

This work was supported by grants from the National Natural Science Foundation of China (31870864), National Key Research and Development Program of China (2018YFA0900404), and China Postdoctoral Science Foundation (2018M641930). We thank Dr. Fajian Hou (Shanghai Institute of Biochemistry and Cell Biology) for generously providing experiment materials and insightful discussions.

AUTHOR CONTRIBUTIONS

Y.S., J.W., T.Z., W.Z., G.S., H.T., and W.D. conducted experiments. N.Q., B.-C.Y., and Y.S. organized the study and prepared the manuscript. All authors discussed the results and commented on the manuscript.

DECLARATION OF INTERESTS

The authors declare no competing interests.

Received: October 26, 2019
Revised: March 8, 2020
Accepted: April 8, 2020
Published: May 22, 2020

REFERENCES

Agarraberes, F., Terlecky, S., and Dice, J. (1997). An intralysosomal hsp70 is required for a selective pathway of lysosomal protein degradation. J. Cell Biol. *137*, 825–834.

Andrews, S., and Rothnagel, J. (2014). Emerging evidence for functional peptides encoded by short open reading frames. Nat. Rev. Genet. *15*, 193–204.

Barbosa, C., and Gene, D. (2014). Upstream open reading frames and human genetic disease (eLS John Wiley & Sons, Ltd).

Boyle, K., and Randow, F. (2013). The role of 'eat-me' signals and autophagy cargo receptors in innate immunity. Curr. Opin. Microbiol. *16*, 339–348.

Brar, G., Yassour, M., Friedman, N., Regev, A., Ingolia, N., and Weissman, J. (2012). High-resolution view of the yeast meiotic program revealed by ribosome profiling. Science *335*, 552–557.

Brubaker, S.W., Gauthier, A.E., Mills, E.W., Ingolia, N.T., and Kagan, J.C. (2014). A bicistronic MAVS transcript highlights a class of truncated variants in antiviral immunity. Cell *156*, 800–811.

Buskiewicz, I., Montgomery, T., Yasewicz, E., Huber, S., Murphy, M., Hartley, R., Kelly, R., Crow, M., Perl, A., Budd, R., et al. (2016). Reactive oxygen species induce virus-independent MAVS oligomerization in systemic lupus erythematosus. Sci. Signal. *9*, ra115.

Calvo, S.E., Pagliarini, D.J., and Mootha, V.K. (2009). Upstream open reading frames cause widespread reduction of protein expression and are polymorphic among humans. Proc. Natl. Acad. Sci. U S A *106*, 7507–7512.

Chatterjee, S., Berwal, S., and Pal, J. (2010). Pathological mutations in 5′ untranslated regions of human genes. In Encyclopedia of Life Sciences (ELS) (Chichester: John Wiley & Sons, Ltd). https://doi.org/10.1002/9780470015902.a0022408.

Fitzgerald, K., McWhirter, S., Faia, K., Rowe, D., Latz, E., Golenbock, D., Coyle, A., Liao, S., and Maniatis, T. (2003). IKKepsilon and TBK1 are essential components of the IRF3 signaling pathway. Nat. Immunol. *4*, 491–496.

Gunišová, S., and Valášek, L.S. (2014). Fail-safe mechanism of GCN4 translational control—uORF2 promotes reinitiation by analogous mechanism to uORF1 and thus secures its key role in GCN4 expression. Nucleic Acids Res. *42*, 5880–5893.

Hou, F., Sun, L., Zheng, H., Skaug, B., Jiang, Q.X., and Chen, Z.J. (2011). MAVS forms functional prion-like aggregates to activate and propagate antiviral innate immune response. Cell *146*, 448–461.

Ishimura, R., Nagy, G., Dotu, I., Zhou, H., Yang, X.L., Schimmel, P., Senju, S., Nishimura, Y., Chuang, J.H., and Ackerman, S.L. (2014). Ribosome stalling induced by mutation of a CNS-specific tRNA causes neurodegeneration. Science *345*, 455–459.

Jacobs, J.L., and Coyne, C.B. (2013). Mechanisms of MAVS regulation at the mitochondrial membrane. J. Mol. Biol. *425*, 5009–5019.

Janich, P., Arpat, A., Castelo-Szekely, V., Lopes, M., and Gatfield, D. (2015). Ribosome profiling reveals the rhythmic liver translatome and circadian clock regulation by upstream open reading frames. Genome Res. *25*, 1848–1859.

Jin, S., Tian, S., Luo, M., Xie, W., Liu, T., Duan, T., Wu, Y., and Cui, J. (2017). Tetherin suppresses type I interferon signaling by targeting MAVS for NDP52-mediated selective autophagic degradation in human cells. Mol. Cell *68*, 308–322.e4.

Johnstone, T., Bazzini, A., and Giraldez, A. (2016). Upstream ORFs are prevalent translational repressors in vertebrates. EMBO J. *35*, 706–723.

Kawai, T., Takahashi, K., Sato, S., Coban, C., Kumar, H., Kato, H., Ishii, K., Takeuchi, O., and Akira, S. (2005). IPS-1, an adaptor triggering RIG-I- and Mda5-mediated type I interferon induction. Nat. Immunol. *6*, 981–988.

Klionsky, D.J., Abeliovich, H., Agostinis, P., Agrawal, D.K., Aliev, G., Askew, D.S., Baba, M., Baehrecke, E.H., Bahr, B.A., Ballabio, A., et al. (2008). Guidelines for the use and interpretation of assays for monitoring autophagy in higher eukaryotes. Autophagy *4*, 151–175.

Kozak, M. (1986). Point mutations define a sequence flanking the AUG initiator codon that modulates translation by eukaryotic ribosomes. Cell *44*, 283–292.

Kozak, M. (1987). Effects of intercistronic length on the efficiency of reinitiation by eucaryotic ribosomes. Mol. Cell Biol. *7*, 3438–3445.

Kozak, M. (1999). Initiation of translation in prokaryotes and eukaryotes. Gene *234*, 187–208.

Kozak, M. (2002). Pushing the limits of the scanning mechanism for initiation of translation. Gene *299*, 1–34.

Lawless, C., Pearson, R.D., Selley, J.N., Smirnova, J.B., Grant, C.M., Ashe, M.P., Pavitt, G.D., and Hubbard, S.J. (2009). Upstream sequence elements direct post-transcriptional regulation of gene expression under stress conditions in yeast. BMC Genom. *10*, 7.

Lee, M.S., and Kim, Y.J. (2007). Signaling pathways downstream of pattern-recognition

receptors and their cross. Annu. Rev. Biochem. *76*, 447–480.

Liang, X., Jackson, S., Seaman, M., Brown, K., Kempkes, B., Hibshoosh, H., and Levine, B. (1999). Induction of autophagy and inhibition of tumorigenesis by beclin 1. Nature *402*, 672–676.

Matsui, M., Yachie, N., Okada, Y., Saito, R., and Tomita, M. (2007). Bioinformatic analysis of post-transcriptional regulation by uORF in human and mouse. FEBS Lett. *581*, 4184–4188.

Mendell, J., Sharifi, N., Meyers, J., Martinez-Murillo, F., and Dietz, H. (2004). Nonsense surveillance regulates expression of diverse classes of mammalian transcripts and mutes genomic noise. Nat. Genet. *36*, 1073–1078.

Meylan, E., Curran, J., Hofmann, K., Moradpour, D., Binder, M., Bartenschlager, R., and Tschopp, J. (2005). Cardif is an adaptor protein in the RIG-I antiviral pathway and is targeted by hepatitis C virus. Nature *437*, 1167–1172.

Minassian, A., Zhang, J., He, S., Zhao, J., Zandi, E., Saito, T., Liang, C., and Feng, P. (2015). An internally translated MAVS variant exposes its amino-terminal TRAF-binding Motifs to deregulate interferon induction. PLoS Pathog. *11*, 1005060.

Mizushima, N., Noda, T., Yoshimori, T., Tanaka, Y., Ishii, T., George, M., Klionsky, D., Ohsumi, M., and Ohsumi, Y. (1998). A protein conjugation system essential for autophagy. Nature *395*, 395–398.

Philo, J., and Arakawa, T. (2009). Mechanisms of protein aggregation. Curr. Pharm. Biotechnol. *10*, 348–351.

Qi, N., Shi, Y., Zhang, R., Zhu, W., Yuan, B., Li, X., Wang, C., Zhang, X., and Hou, F. (2017). Multiple truncated isoforms of MAVS prevent its spontaneous aggregation in antiviral innate immune signalling. Nat. Commun. *8*, 15676.

Randow, F., and Youle, R.J. (2014). Self and nonself: how autophagy targets mitochondria and bacteria. Cell Host Microbe *15*, 403–411.

Ronnblom, L. (2011). The type I interferon system in the etiopathogenesis of autoimmune diseases. Upsala J. Med. Sci. *116*, 227–237.

Seth, R., Sun, L., Ea, C., and Chen, Z. (2005). Identification and characterization of MAVS, a mitochondrial antiviral signaling protein that activates NF-kappaB and IRF 3. Cell *122*, 669–682.

Shao, W., Shu, D.H., Zhen, Y., Hilliard, B., Priest, S.O., Cesaroni, M., Ting, J.P.Y., and Cohen, P.L. (2016). Prion-like aggregation of mitochondrial antiviral signaling protein in lupus patients is associated with increased levels of type I interferon. Arthritis Rheumatol. *68*, 2697–2707.

Sharma, S., tenOever, B., Grandvaux, N., Zhou, G., Lin, R., and Hiscott, J. (2003). Triggering the interferon antiviral response through an IKK-related pathway. Science *300*, 1148–1151.

Shi, Y., Yuan, B., Qi, N., Zhu, W., Su, J., Li, X., Qi, P., Zhang, D., and Hou, F. (2015). An autoinhibitory mechanism modulates MAVS activity in antiviral innate immune response. Nat. Commun. *6*, 7811.

Shibutani, S., Saitoh, T., Nowag, H., Munz, C., and Yoshimori, T. (2015). Autophagy and autophagy-related proteins in the immune system. Nat. Immunol. *16*, 1014–1024.

Sun, L., Wu, J., Du, F., Chen, X., and Chen, Z.J. (2013). Cyclic GMP-AMP synthase is a cytosolic DNA sensor that activates the type I. Science *339*, 786–791.

Takeuchi, O., and Akira, S. (2010). Pattern recognition receptors and inflammation. Cell *140*, 805–820.

Wang, X., and Rothnagel, J. (2004). 5'-untranslated regions with multiple upstream AUG codons can support low-level translation via leaky scanning and reinitiation. Nucleic Acids Res. *32*, 1382–1391.

Wu, B., Peisley, A., Tetrault, D., Li, Z., Egelman, E.H., Magor, K.E., Walz, T., Penczek, P.A., and Hur, S. (2014). Molecular imprinting as a signal-activation mechanism of the viral RNA sensor RIG-I. Mol. Cell *55*, 511–523.

Xu, H., He, X., Zheng, H., Huang, L.J., Hou, F., Yu, Z., de la, C.M., Borkowski, B., Zhang, X., Chen, Z.J., et al. (2014). Structural basis for the prion-like MAVS filaments in antiviral innate immunity. Elife *1*, 01489.

Xu, L., Wang, Y., Han, K., Li, L., Zhai, Z., and Shu, H. (2005). VISA is an adapter protein required for virus-triggered IFN-beta signaling. Mol. Cell *19*, 727–740.

Zandi, E., Rothwarf, D., Delhase, M., Hayakawa, M., and Karin, M. (1997). The IkappaB kinase complex (IKK) contains two kinase subunits, IKKalpha and IKKbeta, necessary for IkappaB phosphorylation and NF-kappaB activation. Cell *91*, 243–252.

Zeng, W., Xu, M., Liu, S., Sun, L., and Chen, Z.J. (2009). Key role of Ubc5 and lysine-63 polyubiquitination in viral activation of IRF3. Mol. Cell *36*, 315–325.

iScience, Volume *23*

Supplemental Information

Upstream ORFs Prevent MAVS Spontaneous Aggregation and Regulate Innate Immune Homeostasis

Yuheng Shi, Jing Wu, Tiansheng Zhong, Wenting Zhu, Guolan She, Hao Tang, Wei Du, Bang-Ce Ye, and Nan Qi

SUPPLEMENTAL ITEMS

■ TRANSPARENT METHODS

Plasmids and antibodies. MAVS cDNA containing 5' UTR were cloned from HEK293T and MEF cells, respectively, and then inserted to pcDNA3.0 vector with the restriction enzyme sites of HindIII and XbaI (namely pcDNA-MAVS-WT and pcDNA-mMAVS-WT). Plasmids encoding various uORFs-deprived mutants, including MAVS-ΔuORF1/2/3/2,3/1,3/1,2/1,2,3 and mMAVS-ΔuORF, were generated by replacing the ATG start condon of uORFs with ATT. Expression vectors for artificial uORF2 were made by insertion of nucleotides "G" or "GC" behind the ATG start condon (See Table. S1). pcDNA-Flag-uORF1/2/3 and pcDNA-uORF1/2/3-GFP were generated by fusing the Flag tag and GFP CDS to the N-terminus and C-terminus of uORFs, respectively. Mutations and deletions were generated by using the Fast-mutagenesis Kit (Catalogue number FM111, TransGen Biotech, Beijing, China) or overlapping PCR strategy. Primers are listed in S2 Table. All constructs were confirmed by DNA sequencing. Autophagy cargo receptors p62, Nix, NDP52, OPTN, NBR1 and TAX1BP1 were described previously (Qi et al., 2017). Commercial MAVS CRISPR Activation Plasmid were purchased from Santa Cruz Biotechnology (sc-400769-ACT). MAVS and uORF2 antibodies were raised by immunizing rabbits with recombinant proteins His-sumo-hMAVS-(aa-301–460) and His-sumo-uORF2, respectively. Commercial antibodies included anti-prohibitin (Abcam, ab75766, dilution 1:10,000), anti-IRF3 (Abcam, 2241-1, dilution

1:3,000), anti-tubulin (Sigma, T5168, dilution 1:7,500), anti-LC3 (Sigma, L8198, dilution 1:3,000), anti-Nix (Abcam, ab8399, dilution 1:1,000), anti-Flag (Sigma, F3165, F7425, dilution 1:5,000), anti-HA (Cell Signaling Technology, 3724S, dilution 1:2,000).

Cells and viruses. HEK293T, *Mavs*$^{-/-}$ 293T, and *Mavs*$^{-/-}$ MEF cell as described (Hou et al., 2011; Shi et al., 2015) were cultured in Dulbecco's modified Eagle's medium (DMEM) medium with 10% fetal bovine serum (FBS, ExCell Bio, FSP500), penicillin (100 U ml^{-1}) and streptomycin (100 mg ml^{-1}). MG132 (S2619), 3-Methyladenine (S2767), chloroquine (S4430) and Bafilomycin A1 (S1413) were purchased from Selleckchem. CCCP (C2759) was purchased from Sigma. Recombinant virus VSV-ΔM51-GFP(Seth et al., 2005) was kindly gifted from Dr. Fajian Hou and used with a multiplicity of infection (MOI)=1. Sendai virus (Cantell strain) from Charles River Laboratories was used at a concentration of 100 HA units ml^{-1}.

Generation of *MAVS* uORFs-deprived HEK293T cell line. The CRISPR/Cas9-mediated genomic knock-in was performed in HEK293T cells to generate *Mavs-(ΔuORF1,2,3)*. Briefly, two CRISPR/Cas9 vectors(Ran et al., 2013) were constructed for creating a double-stranded break targeted the first exon (harboring uORF1 and uORF2) and the second exon (harboring uORF3) of the human *MAVS* gene, respectively. The donor plasmids, which contained

sequences flanking the target exons and harbored a mutation for replacing ATG start codons with ATT, were generated for homologous recombination. The Cas9 vectors and the donor DNA were co-transfected into HEK293T cells using Lipo 2000 (11668019, Invitrogen). Two weeks after puromycin resistance selection, individual cellular colonies were picked from 96 well plate. Extract the genomic DNA and then sequenced to verify modification on the *MAVS* gene. Oligonucleotides are listed in Table. S2.

Immunoprecipitations. HEK293T cells were transfected with indicated constructs. Thirty-six hours after transfection, cells were harvested and resuspended in lysis buffer [HEPES 20 mM pH 7.5, $MgCl_2$ 5 mM, KCl 10 mM, EGTA 0.5 mM, Triton X-100 1%, and 1% protease inhibitor cocktail (Roche)]. Following a brief centrifugation, the supernatant were incubated with anti-HA agarose beads (26181, Thermo) at 4°C for 4 h. After incubation, HA beads were spun down and washed for three times with lysis buffer. The binding products were subjected to SDS-PAGE and immunoblotting analysis.

Quantitative PCR. Total RNA was extracted from cells using RNA simple total RNA kit (DP419, Tiangen, Shanghai, China), and then reversed transcribed by using the GoScript™ Reverse Transcription system (A5000, Promega). As templates, cDNAs were subjected to qPCR assay using SuperReal Premix Plus (FP205, Tiangen). Data was normalized by the level of GAPDH expression in

each individual sample. The $2^{-\Delta\Delta Ct}$ method was used to calculate gene relative expression. Primers are listed in Table. S2.

Subcellular fractionation and *in vitro* IRF3 activation assay. Subcellular fractionation was performed as described previously (Shi et al., 2015). In brief, cells were homogenized in hypotonic buffer [10 mM Tris-Cl (pH 7.5), 10 mM KCl, 1.5 mM $MgCl_2$ and 0.5 mM EGTA], and the lysate were then centrifuged at 4°C, 1,000 g for 5min to get the supernatant (S1). S1 was further centrifuged at 4°C, 10,000 g for 10 min to separate the supernatant (S5) and pellet (P5). Subsequently, S5 was concentrated at 4°C, 100,000 g for 30 min, and the resultant supernatant (S100) was collected. P5 fractions containing the crude mitochondria and S100 were used for the *in vitro* IRF3 activation assay as described (Shi et al., 2015).

Semidenaturing detergent agarose gel electrophoresis. First, isolated pellets containing crude mitochondria from HEK293T cells, and then resuspended the pellet in the SDD loading sample buffer (0.5×TBE, 10% glycerol, 2% SDS and 0.0025% bromophenol blue). After loading onto a vertical 1.5% agarose and gel electrophoresis in the running buffer (1×TBE and 0.1% SDS) for 30 min with a constant voltage of 100V at 4°C, immunoblotting was performed.

Fluorescence microscopy. Cells indicated in the paper were infected with VSV-ΔM51-GFP (MOI=1) in order to examine VSV proliferation. Eight hours after infection, the fluorescence intensity was observed. All the images were taken by Olympus IX71 inverted fluorescence microscope.

ELISA. Concentrations of the cytokine in cell culture supernatants were measured by IFN-BETA Mouse ELISA Kit (High Sensitivity, PBL Assay Science) according to the manufacturer's instructions.

Plaque assay. Plaque assay was performed as described previously(Qi et al., 2017). In brief, cells were infected with VSV at MOI=1. Twelve hours post infection, aliquots of culture media containing recovered VSV were collected, and then infected HEK293T cells in 6-well plates with serial dilutions for 1 h. The infected cells were covered with 1% soft agar dissolved in DMEM containing 5% FBS and incubated for 48 h. Plates were stained with 0.1% crystal violet in DMEM to display plaques, which were then quantitated.

Flow cytometric analyses. Mitochondrial mass was measured by fluorescence levels. The cells were stained with 200 nM MitoTracker^{TM} Green FM and 150 nM MitoTracker^{TM} Red CMXRos (M7514 and M7512, Thermo Fisher Scientific) at 37°C for 20 min. Cells were washed with PBS, trypsinized and then resuspended in PBS for FACS analysis. Mitochondria associated ROS

was measured using the ROS assay kit (C1300, APPLYGENE, Beijing, China) according to manufacturer's instructions. FACS data were collected using BD LSR II Flow Cytometer (BD Biosciences, New Jersey, USA), and analyzed by software FlowJo version 7.6.1.

Treatment with shRNA. Vectors encoding shRNAs were constructed based on pLKO.1. Sequences of targeting genes can be found in S2 Table. In brief, cells seeded into 6-well plates or 10-cm dishes were transfected with indicated shRNA vectors using Lipofectamine 2,000 (Invitrogen). Thirty-six hours post transfection, the second transfection were taken at the same condition. Cells were collected at 36 h after the second transfection for the following assays.

Statistical analysis. All data are presented as mean values ±s.d. on the basis of at least three independent experiments. Statistical significance between two groups was determined by unpaired two-tailed Student's t-test. Differences were considered to be significant when $P<0.05$. Quantification of the protein band intensity was performed using Quantity One imaging software (Bio-Rad Laboratories, USA).

■ FIGURES

Figure. S1

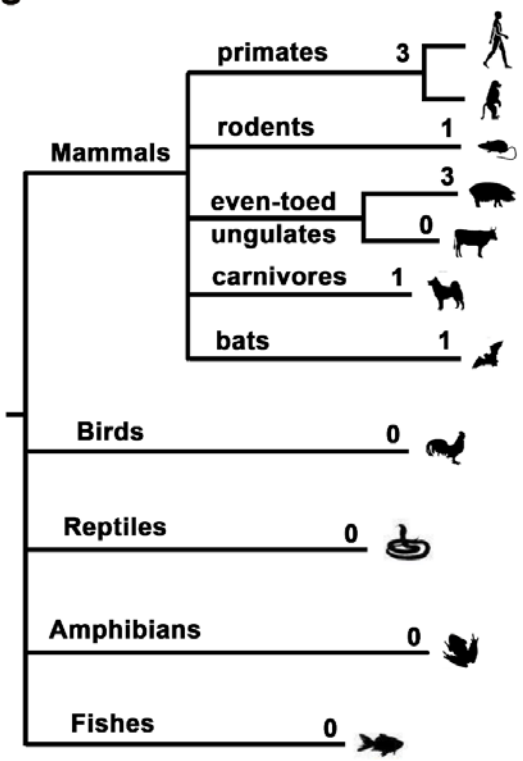

Figure S1. Abundance of uORF in the *MAVS* gene from vertebrates, Related to Figure 1. Representative species of diverse taxonomic groups in vertebrates are listed, with their *MAVS* transcripts subjected to uORF analysis. To reduce stochastic noise, the reading frames containing at least six codons (≥21 nucleotides in length) in the 5' UTR are identified as uORF. The GenBank accession numbers of analyzed *MAVS* transcripts from diverse species are listed as follows: *Danio rerio* (NM_001080584.2), *Xenopus tropicalis* (XM_018090897.1), *Pseudonaja textilis* (XM_026718946.1), *Gallus gallus* (NM_001012893.1), *Pteropus Alecto* (XM_006921628.3), *Canis lupus familiaris* (XM_014106837.2), *Bos taurus* (NM_001046620.2), *Sus scrofa* (XM_021077145.1), *Tupaia belangeri* (KM005100.1), *Mus musculus* (NM_001206383.1), *Pan troglodytes* (XM_024352162.1), *Homo sapiens* (NM_020746.5).

Figure S2

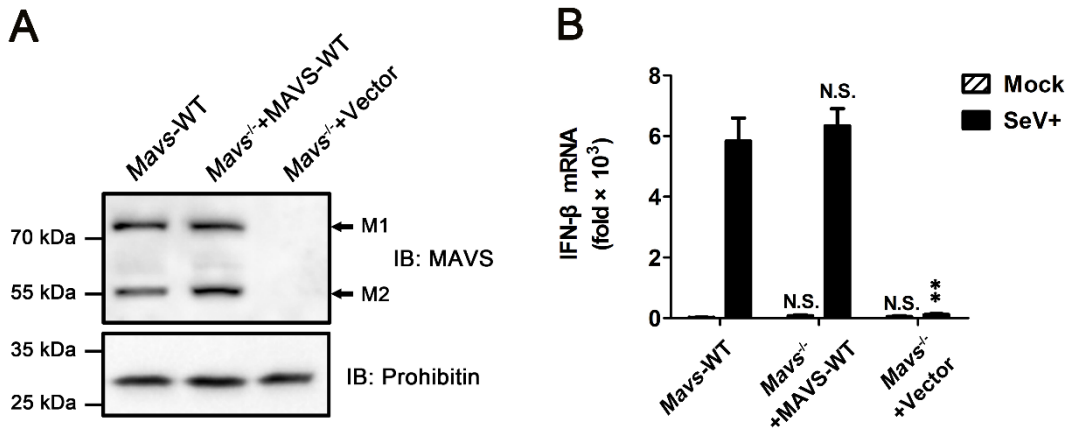

Figure S2. A cellular model for studying the function of MAVS in a near-physiological condition, Related to Figure 1.

In parallel with wildtype HEK293T cells (*Mavs*-WT), recovery of MAVS-WT in *MAVS*-deficient (*Mavs*$^{-/-}$) cells produces MAVS at a near-endogenous level (A), and induces the IFN-β expression under SeV-stimulation (B). *Mavs*$^{-/-}$ cells were transfected with MAVS-WT or empty vector for thirty-six hours. Twenty-four hours after transfection, cells were infected with or without Sendai virus. Cells were harvested at twelve hours post-infection. P5 fractions were isolated and used to analyze the MAVS protein level by immunoblotting with anti-MAVS antibody. RNA was extracted and qPCR was performed to measure IFN induction. The results show means ± SDs (n=3, $^{**}p < 0.01$, N.S., non-significant; t test).

Figure S3

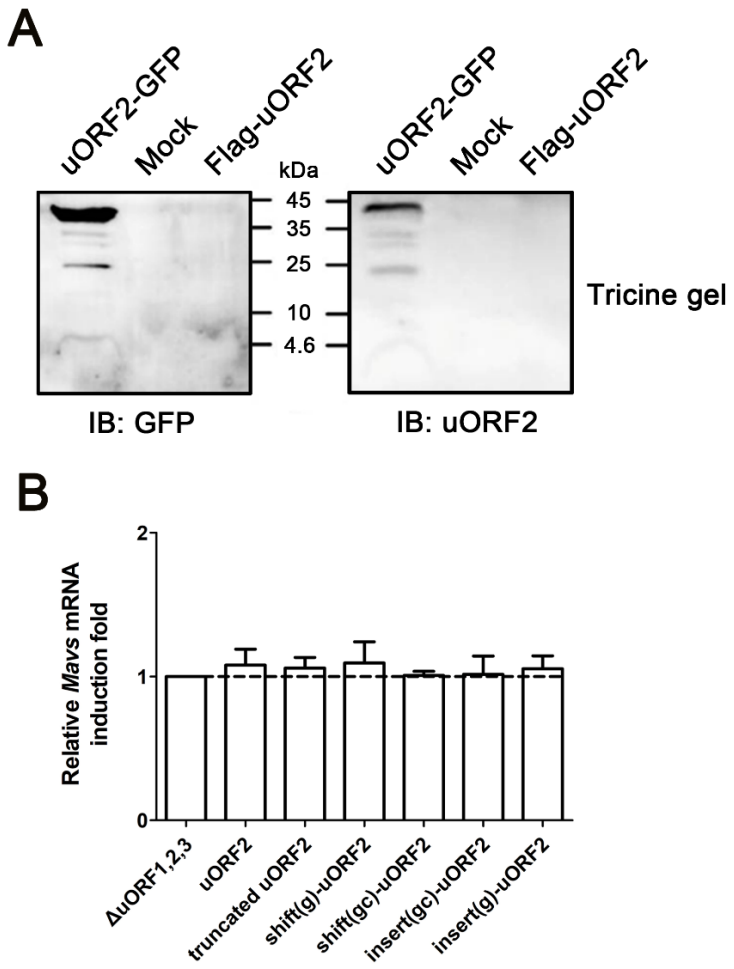

Figure S3. The protein level of *MAVS* uORF2-translated peptide in HEK293T cells, Related to Figure 4.

(A) Immunoblotting analysis showing that *MAVS* uORF2 cannot translate a peptide. For analyzing the translation of uORF2, whole cell lysates obtained from wildtype HEK293T cells untransfected, or transfected with uORF2-GFP and Flag-uORF2 for thirty-six hours were subjected to immunoblotting using anti-uORF2 and anti-GFP antibodies. (B) Relative quantification of mRNA induction showing that insertion and mutation at uORF2 AUG codon do not influence the *MAVS* mRNA level. Transfection was performed as described in Figure 4D. After cells were harvested, RNA was extracted and qPCR was performed to measure the *MAVS* mRNA induction. The results show means ± SDs (n=3, $^{**}p < 0.01$; t test).

Figure S4

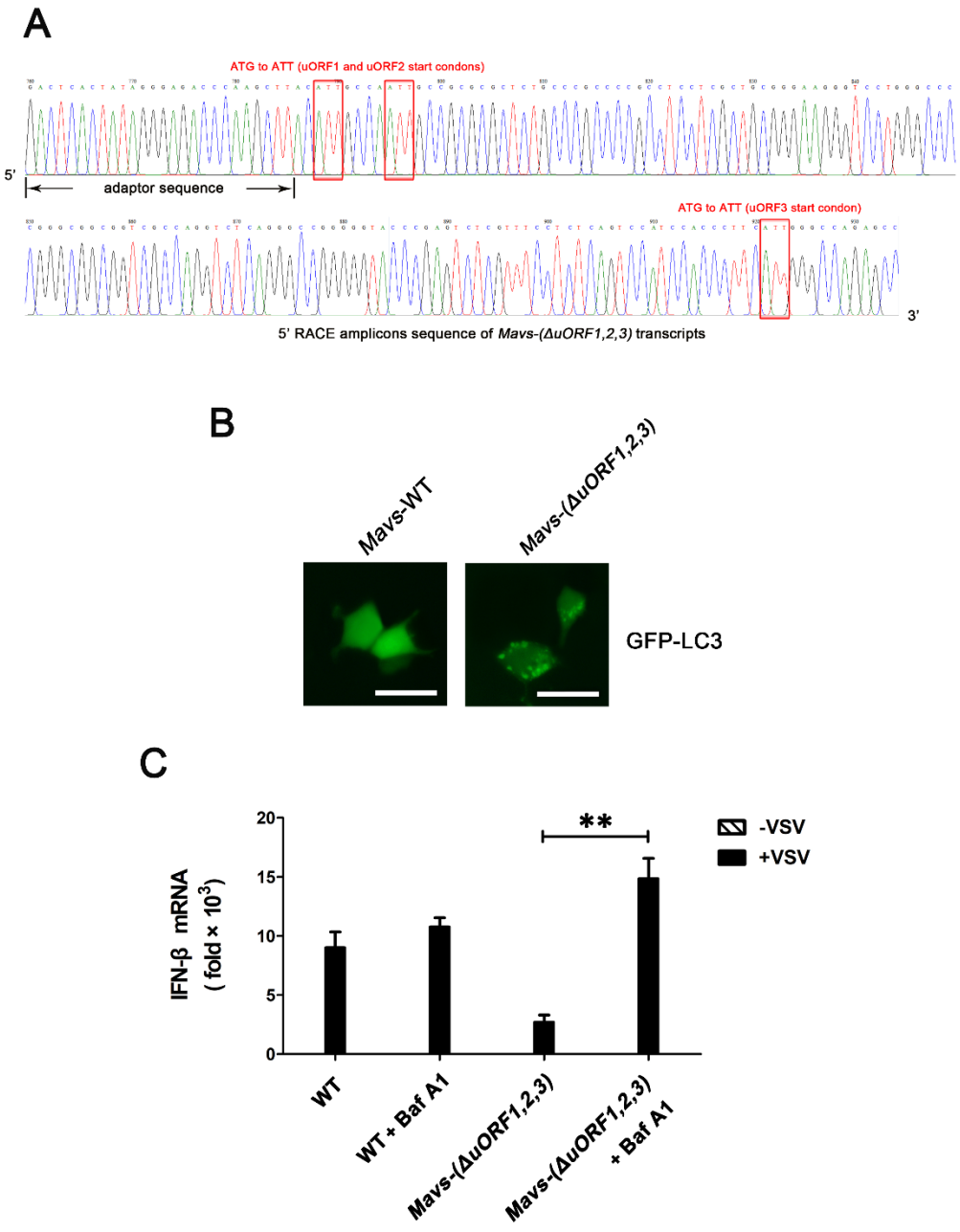

Figure S4. Generation and characterization of the Mavs-(ΔuORF1,2,3) cell line, Related to Figure 5.

(A) Sequencing of the 5' RACE amplicons from the *MAVS* transcripts in *Mavs-(ΔuORF1,2,3)* cells. (B) Fluorescent microcopy imaging of WT and *Mavs-(ΔuORF1,2,3)* HEK293T cells transfected with GFP-LC3, as described in Figure 5E. Scale bar represents 20 micrometers. (C) Treatment with the autophagy inhibitor Baf A1 rescues the antiviral capability of endogenous MAVS-(ΔuORF1,2,3), related to Figure 5G. *Mavs-(ΔuORF1,2,3)* and wildtype HEK293T cells were treated with or without 0.2 μM Baf A1 for six hours before infection with VSV (MOI=1). Twelve hours post infection, RNA was extracted and qPCR was performed to measure the IFN induction. The results show means ± SDs (n=3, $^{**}p < 0.01$; t test).

Figure S5

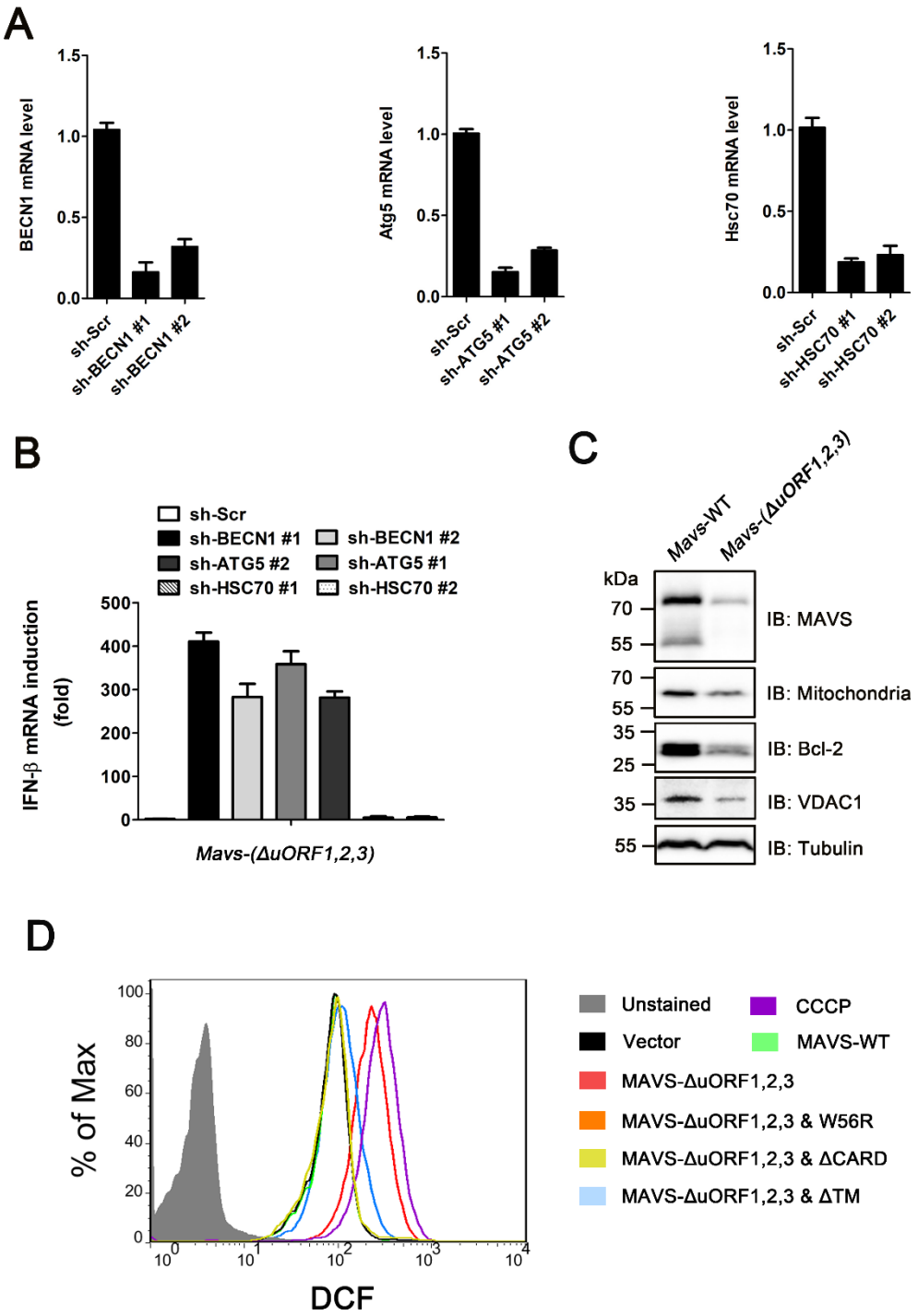

Figure S5. Spontaneously-aggregated MAVS induced by endogenous or artificial lacking-uORFs expression provokes mitophagy in cells, Related to Figure 6.

(A) qPCR showing the knock-down efficiency of Beclin 1 and ATG5 by indicated shRNAs at mRNA level. *Mavs-(ΔuORF1,2,3)* cells were treated with shRNAs as described in Figure 6A. The results show means ± SDs (n=3). (B) Knockdown of Beclin 1 and ATG5 rather than HSC70 stimulates the IFN expression in *Mavs-(ΔuORF1,2,3)* cells. Treatment were performed as described in Figure 6A. Thirty-six hours post transfection, cells were subjected to RNA

extraction and qPCR for measuring the IFN induction fold. The results show means ± SDs (n=3). (C) Immunoblotting to show that mitochondrial turnover was induced in *Mavs-(ΔuORF1,2,3)* cells. Protein levels of total mitochondria, as well as the outer membrane proteins Bcl-2 and VDAC1 were determined. Tubulin was used as loading control. (D) HEK293T *Mavs*$^{-/-}$ cells untreated or transfected with empty vector, MAVS-WT or its mutants as indicated were collected for FACS analysis to determine the ROS production. CCCP treatment was analyzed as positive control. Histograms of FACS analysis are depicted.

Figure S6

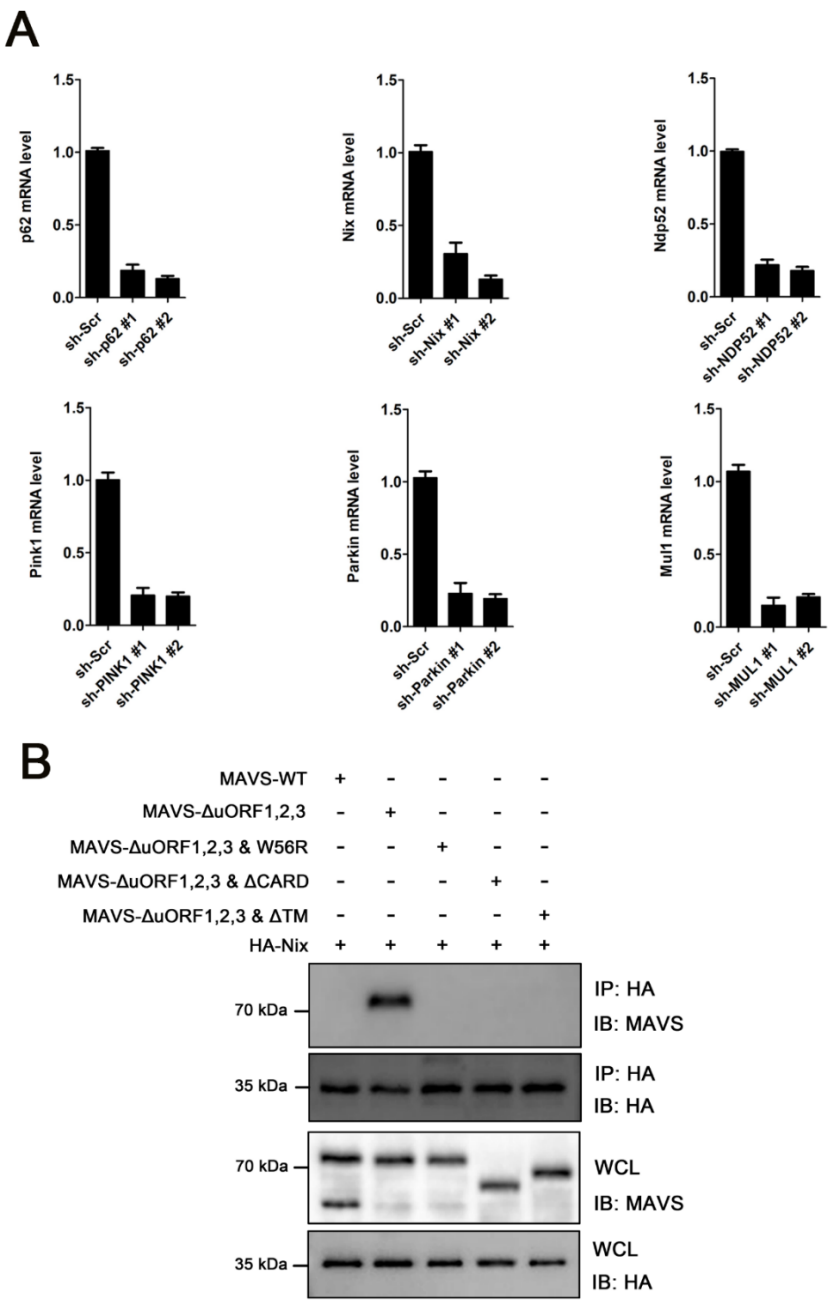

Figure S6. Efficiency of shRNA-mediated knockdown and the interaction between Nix and various MAVS mutants, Related to Figure 6.

(A) qPCR showing the knock-down efficiency of p62, Nix, NDP52, PINK1, Parkin and MUL1 by indicated shRNAs at mRNA level. *Mavs-(ΔuORF1,2,3)* cells were treated with indicated shRNAs as described in Figure 6E. The results show means ± SDs (n=3). (B) HA-Nix were transfected into HEK293T *Mavs*$^{-/-}$ cells together with plasmids encoding MAVS-WT and various mutants as indicated. Thirty-six hours after transfection, cells were harvested and subjected to immunoprecipitation and immunoblotting.

■ TABLES